# A rapid transfer of virions coated with heparan sulfate from the ECM to cell surface CD151 defines a step in the human papillomavirus infection cascade

Annika Massenberg[1], Yahya Homsi[1], Carl Niklas Schneider[1], Snježana Mikuličić[2], Tatjana Döring[2], Luise Florin[2,3,*], Thorsten Lang[1,*]

[1]University of Bonn, Faculty of Mathematics and Natural Sciences, Life & Medical Sciences (LIMES) Institute, Carl-Troll-Straße 31, 53115 Bonn, Germany
[2]Institute for Virology, University Medical Center of the Johannes Gutenberg-University Mainz, Obere Zahlbacher Straße 67, 55131 Mainz, Germany
[3] Research Center for Immunotherapy (FZI), University Medical Center of the Johannes Gutenberg-University Mainz, 55131 Mainz, Germany

*Correspondence should be addressed to Thorsten Lang (thorsten.lang@uni-bonn.de) or Luise Florin (lflorin@uni-mainz.de)

Keywords: virus infection, primary attachment site, secondary receptor, heparan sulfate, filopodia, transport

**Abstract**

Human Papillomaviruses (HPVs) are the underlying cause of several types of cancer though they are mostly known for their association with cervical carcinoma. Before establishing an infection, the virions must reach their target cells through a break in the epithelial barrier. After binding to heparan sulfate (HS) of the extracellular matrix (ECM), they translocate to the cell surface and co-internalize with the entry factor CD151.

For studying these early events of the infection cascade, we block the translocation from ECM-attachment sites to the cell body, release the block, and monitor the association of virions with CD151 or HS. We observe quick virion translocation from the ECM to the cell body within 15 min. During this process, virions associate with the tetraspanin CD151 present at the cell border or at filopodia. Translocating virions are decorated with HS, which they lose in the next few hours, presumably prior to endocytosis.

Our observations reveal a rapid step in the HPV infection cascade: the transfer of HS-coated virions from the ECM to CD151. This step is too fast to account for the asynchronous uptake of HPVs which is likely driven by glycan-processing and HS uncoating contributing to virus structural activation in preparation for endocytosis.

## Introduction

Already in the 80s, Harald zur Hausen proposed a role of human papillomaviruses in cancer (***zur Hausen, 2009***). Since then, five more classes of oncogenic viruses have been identified (***Galati et al., 2024a***). To date, it is assumed that more than 10% of the worldwide human cancer burden is associated with infectious agents (***Galati et al., 2024a***), from which about a half is caused by *Papillomaviridae* (***Martel et al., 2017***) For this reason, the understanding of viral entry strategies has implications going beyond the classical treatment of acute viral infections.

Human papillomaviruses are small, non-enveloped viruses with a diameter of ~55 nm. The icosahedral capsid is mainly composed of pentameric L1 capsomers. Together with fewer L2 capsid proteins, capsomers surround a histone core bearing a circular double-stranded DNA (***Baker et al., 1991; Ozbun and Campos, 2021***). From the more than 200 phylogenetically classified HPV genotypes, the most oncogenic ones are HPV16 and HPV18 (***Galati et al., 2024b***), which are responsible for about 70-80% of the cervical cancer cases (***Christiansen et al., 2015***). In addition, they cause other severe cancers such as anogenital, head and neck tumors (***Doorbar et al., 2012***).

Papillomavirus infection requires a break in the epithelial barrier, through which virions reach mitotically active basal cells of the epithelia (***Ozbun and Campos, 2021***). Here, virions bind to the linear polysaccharide heparan sulfate (HS) that is an important constituent of the extracellular matrix (ECM) and the plasma membrane. In the latter case, it is attached to membrane proteins, so called heparan sulfate proteoglycans (HSPGs). Positively charged and polar residues of the L1 capsid protein interact with negative charges of HS, resulting in a strong bond (***Dasgupta et al., 2011; Giroglou et al., 2001; Joyce et al., 1999; Knappe et al., 2007; Surviladze et al., 2015***). While in cell culture virions bind to HS of the cell surface and the ECM, it has been suggested that *in vivo* they bind predominantly to HS of the extracellular basement membrane (***Day and Schelhaas, 2014; Kines et al., 2009; Schiller et al., 2010***).

Regardless of where the virions bind to HS, they must detach from the linear polysaccharide before they bind to cell surface receptors and are internalized (***Ozbun and Campos, 2021***). However, the strong electrostatic bonds do not allow for HS-virion dissociation. Two release mechanisms are discussed, that mutually are not exclusive. In one model, binding to HS structurally results in capsid enlargement and softening (***Feng et al., 2024***), finally resulting in the exposure and cleavage of capsid proteins (***Becker et al., 2018***), which is required for further steps in infection. In an alternative model, the direct HS-virion bond remains. However, cleavage of HS/HSPGs by proteinases and heparanases produces fragmented HS that, albeit still bound to the virion surface, no longer immobilizes the virion (***Surviladze et al., 2012; Surviladze et al., 2015***).

72 Once the virions are released, they could reach the cell surface simply by passive diffusion. In
73 a co-culture trans-well assay, PsVs from donor cells infect spatially separated receiver cells (***Surviladze***
74 ***et al., 2012***), demonstrating that free diffusion of virions is sufficient for infection. However, an active
75 transport mechanism has been reported as well. PsVs migrate along actin-rich protrusions from the
76 ECM towards the cell body (***Schelhaas et al., 2008; Smith et al., 2008***).
77 While it is generally agreed on that HS is a primary virion attachment site, the molecular
78 identity of the receptor complex on the cell surface is unknown. This complex is most likely a
79 multimeric complex rather than a single molecular component. Possible candidates are proteins
80 crucial for cell entry, as the tetraspanin CD151 (***Mikuličić et al., 2019; Scheffer et al., 2013; Spoden et***
81 ***al., 2008***), integrin-α6 (Itgα6) (***Evander et al., 1997; Yoon et al., 2001***), growth factor receptors
82 (***Mikuličić et al., 2019; Surviladze et al., 2012***), and the annexin A2 heterotetramer (***Dziduszko and***
83 ***Ozbun, 2013; Woodham et al., 2012***). From these molecules, the tetraspanin CD151 could play a
84 coordinating role, as tetraspanins have been suggested to organize viral entry platforms in several
85 types of viral infections, including infections with coronavirus, cytomegalovirus, hepatitis C virus,
86 human immunodeficiency virus, human papilloma virus, and influenza virus (***Bruening et al., 2018;***
87 ***Earnest et al., 2015; Florin and Lang, 2018; Hantak et al., 2019; Hochdorfer et al., 2016; Scheffer et***
88 ***al., 2013; Zona et al., 2013***). Tetraspanin entry platforms could form in a slow and stochastic manner,
89 providing an explanation for the asynchronous virion uptake with half-times of above 10 h (***Becker et***
90 ***al., 2018***). However, it is unclear whether virions associate with CD151 already during virion transfer
91 from the ECM to the cell surface, or perhaps much later, in preparation of the endocytic uptake.
92 In this study, we explore the actin-dependent transport of HPV-PsV infection by employing
93 the cell permeable mycotoxin and actin polymerization inhibitor cytochalasin D (CytD). We find that
94 CytD causes the trapping of HPV16 pseudovirions (PsVs) in the ECM, where they remain accumulated
95 adjacent to the cell periphery. Upon CytD removal, HS-decorated PsVs move from the ECM to cell
96 surface CD151. The association of PsVs with CD151 persists within the next few hours, whereas the
97 HS coat is stripped off. These findings distinguish a step in the infection cascade with CD151 playing
98 an early role directly after the release of virions from the ECM.
99
100
101 **Results**
102 *Cytochalasin D arrests the transfer of PsVs from the extracellular matrix to the cell surface*
103 The molecular surface of PsVs is immunologically indistinguishable from HPV virus particles
104 (***Doorbar et al., 2012***), which makes them a widely used tool for studying host cell entry. In this study,
105 we employ HPV16-pseudovirions with an encapsidated luciferase reporter-plasmid under the control
106 of the HPV16-promotor. Instead of viral-DNA, a luciferase-encoding plasmid enters the nucleus,

107 enabling the analysis of the infection rate via the luciferase activity. Additionally, the plasmids are
108 composed of nucleotides to which fluorophores can be coupled by click-chemistry. This allows for
109 their detection by fluorescence microscopy throughout the entire infection pathway.

110 Many PsVs in the ECM are too far away from the cell surface to allow for direct physical
111 contact between PsVs and entry receptors. In order to reach the cell surface, virions migrate by an
112 actin-dependent transport along cell protrusions towards the cell body (***Schelhaas et al., 2008; Smith***
113 ***et al., 2008***). We aimed for blocking this transport in HaCaT cells, a human keratinocyte cell line that
114 is widely used as a cell culture model for HPV infection. Cells are incubated for 5 h with PsVs in the
115 absence or presence of 10 µg/ml CytD. Previously, it has been shown that this CytD concentration
116 stops cell migration only after a few minutes (***Peng et al., 2011***). Therefore, we assume that CytD does
117 not immediately stop PsV translocation. Figure 1A shows cells that, after the 5 h incubation, are fixed
118 and stained by a membrane marker (the dye TMA-DPH) to mark the main cell body (gray), for PsVs (by
119 click-chemistry; magenta), HS (antibody staining; cyan), and the membrane protein Itgα6 (antibody
120 staining; green). In the control, PsVs frequently locate within the area of the cell body (Figure 1A,
121 upper row; see outline based on TMA-DPH staining). In contrast, when CytD was present, the cell body
122 is largely devoid of PsVs (Figure 1A, lower row; please note that the brightness in the center is mainly
123 caused by autofluorescence). Instead of being transported to the cell body as in the control, PsVs
124 accumulate adjacent to the cell body. This region is likely to be the ECM as it is up to several µm wide
125 and rich in HS. We conclude that, upon inhibition of actin-dynamics by CytD, PsVs remain accumulated
126 in the ECM, that in this assay is clearly distinguishable from the cell body.

127 Comparing the total PsV intensities in the upper (control) and lower (CytD) magenta panels in
128 Figure 1A suggests that the amount of accumulated PsVs at the periphery does not differ greatly from
129 the amount of PsVs in the control. This is surprising, as CytD should not inhibit enzymes involved in
130 capsid- or HS/HSPGs-processing, which is supposedly sufficient for the release of PsVs. Therefore, we
131 conclude that potentially releasable PsVs remain in association with the ECM or the cell body.
132 However, a quantitative comparison is not possible in this experiment because of the central
133 autofluorescence (Figure 1A, large magenta area in the center) overlapping with some of the PsVs. For
134 that reason, we employed unroofed cells (***Heuser, 2000***), also called membrane sheets. After
135 treatment of cells with PsVs and CytD as above, membrane sheets are generated by brief ultrasound
136 pulses that remove the upper cellular parts (and thus any intracellular autofluorescence), leaving
137 behind the extracellular matrix and the basal membrane along with the bound PsVs. During imaging,
138 membrane sheets are identified via staining of F-actin with fluorescent labelled phalloidin (Figure 1B,
139 green). As in the experiment above (Figure 1A), PsVs remain accumulated after CytD treatment,
140 adjacent to the now isolated basal membrane (Figure 1B, magenta).

141 The PsV maxima density (Figure 1B, magenta, detected as local maxima of antibody stained
142 L1) and the PsV intensity are quantified in an area covering the cell body and the periphery. Compared
143 to the control, CytD reduces the PsV maxima density by ~ 30% (the PsV maxima density in the control
144 and CytD treated cells is 0.7 and 0.5 PsVs/$\mu m^2$, respectively), whereas the maxima intensity increases
145 by ~ 40% (Figure 1C). A histogram of the PsV maxima intensities illustrates that CytD broadens the
146 intensity distribution towards many PsVs that are several-fold brighter than the most frequent maxima
147 intensity of the control (Figure 1D). Brighter PsVs resulting from CytD treatment can also be seen in
148 the L1 images of Figure 1B (shown at the same scaling). We assume that this observation is due to the
149 limited microscopic resolution, as CytD is unlikely to act directly on PsVs (e.g. by fusing them to larger
150 and brighter particles). The accumulation of PsVs results in overlapping and thus poorly resolved
151 maxima which are ~ 40% brighter but of which there are ~ 30% fewer. The decrease in maxima density
152 is in the range of the increase in intensity, which yields a similar total signal in both conditions.
153 We addressed whether PsVs would still be accumulated when adding CytD 1 h after adding
154 the PsVs rather than simultaneously (Figure 1B, lower panel, CytD after 1 h). As in the CytD condition,
155 we see accumulated PsVs adjacent to the isolated basal membrane (Figure 1B, arrows point towards
156 PsV accumulations). Furthermore, we find a broader PsV maxima intensity distribution compared to
157 the control but a narrower intensity distribution compared to the sample where CytD is present during
158 the entire 5 h incubation (Figure 1D). We conclude that without CytD it takes longer than 1 h for the
159 PsVs to be translocated to the cell body. However, the preparation of PsVs for the translocation step
160 likely is completed after 5 h.
161 Hence, it appears that CytD only arrests PsVs on their journey towards the cell surface.
162 However, our assay is not very precise, and we do not know how many PsVs in the control were
163 already endocytosed, which would reduce the reference value. Therefore, we can only say that within
164 the 5 h incubation period we do not lose a major part of accumulated PsVs after processing in the
165 ECM.
166
167 *The blocking of PsV endocytosis by cytochalasin D is reversible*
168 CytD not only arrests the transport of PsVs to the cell but is known to block other actin-
169 dependent processes, which strongly affects the physiology of the cell. Therefore, we investigated
170 whether PsVs would proceed normally on their infection pathway, after removal of CytD. In order to
171 allow for recovery from CytD, cells were washed after the 5 h PsV/CytD treatment, then incubated for
172 another 19 h and the infection rate was subsequently determined by measuring the luciferase activity
173 in the cell lysate. Compared to the control, CytD reduced luciferase activity by 30% (Figure 1E; left). A
174 certain degree of reduced infectivity is to be expected, as PsVs have ~20% less time to complete

175 infection as compared to PsVs infecting cells that were not treated with CytD. When PsVs were not
176 washed off and incubated for 24 h (5 h + 19 h), the infection rate increased by 50 %, whereas
177 continuous treatment with CytD results in no infection (Figure 1E; right). The latter is in line with
178 previous studies (***Schelhaas et al., 2008; Selinka et al., 2002; Selinka et al., 2007; Spoden et al., 2013***)
179 showing that CytD is a strong inhibitor of HPV infection. In any case, PsVs proceed on the infection
180 pathway when CytD is removed. The reduced infection rate of 30% can be explained, at least in part,
181 by the 5 h delay by which PsVs reach the cell surface. Therefore, we propose that CytD is suitable for
182 transiently arresting PsVs in a state between primary attachment to HS and cell surface binding.
183
184 *The transfer of PsVs from the ECM to the cell body is fast and efficient*
185 Next, we studied the time course of PsV translocation. Cells were treated as in Figure 1A (in
186 Figure 2 the 0 min time point is identical), followed by washing off of PsVs/CytD and fixation after 0,
187 15, 30 and 60 min. The integrated density of PsVs locating at the cell periphery (Figure 2A, the cell
188 periphery is defined by the white lines) is quantified and plotted against time. Compared to the
189 control, CytD treatment results in a 6-fold increase of PsVs in the periphery when cells are immediately
190 fixed after washing off of CytD (0 min time point). This increase is more than halved when cells were
191 incubated for another 15 min after washing off of CytD and after 30 min, the level of the control is
192 reached (Figure 2B). Hence, the half-time of PsV translocation from the periphery to the cell body is
193 about 15 min, demonstrating that translocation is fast and efficient. Considering the fact that prior to
194 endocytosis virions remain several hours on the cell surface, the duration of translocation is short,
195 making it unlikely that it contributes to the asynchronous virion uptake that is observed for HPV-PsVs.
196
197 *Translocation of PsVs to CD151*
198 As shown above, after CytD removal, the accumulated PsVs approach the cell surface. During
199 this process, they may be coated with ECM cleavage products, and at some point, bind to cell surface
200 HPV entry factors, like the tetraspanin CD151. For studying these events in detail, we employ
201 superresolution STED microscopy, analyzing the association of PsVs with HS and CD151 over time.
202 Cells are treated and monitored as in Figure 2, but with an extended time window of up to 180 min,
203 as cell surface processes are expected to take longer than an hour.
204 After fixation, PsVs and CD151 were double-stained with antibodies against L1 and CD151,
205 without prior cell permeabilization (cell surface staining, albeit fixation perforates the cell membrane
206 to some extent). In addition, we stained F-actin with fluorescent labelled phalloidin. We
207 simultaneously image L1 and F-actin in the confocal and CD151 in the STED channel.
208 As shown in Figure 3A, CD151 concentrates in spots scattered across the cell surface. It is also
209 present at cell protrusions that are rich in F-actin and vary strongly in number and shape (Figure 4A

210 shows anecdotal images of these filopodia). The antibody staining against PsVs, like the PsV click-
211 chemistry staining in Figure 1A and 2A, is highly variable. CytD conserves the accumulated PsVs at the
212 cell periphery and at early time points PsVs appear brighter (Figure 3A). Similar to Figure 2, we
213 analyzed the time course of the diminishment of accumulated PsVs but focused on PsVs that are very
214 close to or have already approached the cell surface (Figure 4B and C, for details see Figure legend of
215 4B). Moreover, we counted the number of PsVs instead of measuring the integrated density. As shown
216 in Figure 4C, the PsVs accumulated in the cell border region diminish with about the same rate as PsVs
217 in the periphery (Figure 2B).

218 Just like the L1 staining of PsVs, the intensity of the CD151 staining between cells is highly
219 variable (Figure 3A and B). In the control, the mean intensity does not change over the 180 min time
220 course, whereas a trend towards a lower mean intensity is observed in the cells treated with CytD,
221 with the last time point being significantly lower than the control (Figure 3B). The decrease of the
222 CD151 staining intensity points towards the possibility that after CytD wash off some CD151 is
223 internalized, presumably due to co-internalization with endocytosed PsVs. This idea is supported by
224 the observation that in particular at 180 min/CytD we observe occasionally CD151/PsV
225 agglomerations (Figure 3A, see structures marked by arrows at 180 min/CytD, for more examples see
226 Supplementary Figure 1A). We did not study this issue systematically, but some of these structures
227 have clear three-dimensional extension (see Supplementary Figure 1B for axial scans) and therefore
228 likely are tubular structures filled with several PsVs, as previously described by electron microscopy
229 (***Schelhaas et al., 2012***). We found fewer of such structures at 180 min/control, as cells might have
230 been actively interacting with PsVs for altogether 8 h, opposed to 3 h in the CytD treated cells. Hence,
231 in the control, PsV endocytosis is less synchronized compared to CytD and therefore we do not find a
232 notable CD151 diminishment.

233 For studying the association between PsVs (L1) and CD151, the Pearson correlation coefficient
234 (PCC) between the channels is calculated. In theory, the PCC would equal 1 in the case of a perfect
235 overlap and -1 for an image and its negative. We should not obtain large PCC values, as in most images
236 PsVs are less abundant than CD151. As expected, the PCCs are around 0.1, with the exception of the
237 0 min/CytD value that is significantly lower and even slightly negative (Figure 3C, for control PCC values
238 of flipped images see Supplementary Figure 2). This reflects the partially mutual exclusion of the two
239 stainings; PsV accumulations are at the cell periphery and the CD151 staining is mainly at the cell body.
240 At 30 min/CytD, the PCC has reached the level of 0.1 as in the other conditions, in line with Figure 2B
241 showing that the accumulated PsVs diminish within 15 min.

242 PsV translocation to the cell surface should increase the number of PsVs that are tightly
243 associated with CD151. As criteria for tight association, we define a distance of 80 nm between PsV

244 and CD151 maxima, a value which is close to the resolution limit of the used microscope (***Finke et al.,***
245 ***2020***). In the control, the fraction of PsVs tightly associated with CD151, after correction for random
246 background association (see Supplementary Figure 3) is about 10% (Figure 3D, control). At 0 min/CytD,
247 we start with a fraction of 5.5%, a value that more than doubles in the next 60 min, although these
248 changes are not significant (Figure 3D, CytD).

249 In summary, we conclude that within 180 min after a 5 h pre-incubation with PsVs (Figure 3D,
250 control) around 10% of the PsVs associate tightly with CD151, with no trend towards more/less
251 association over time. With the exception of the lower 0 min/CytD value of 5.5%, CytD has no effect
252 on the association (Figure 3D, CytD). The 0 min/CytD value could be an underestimation, because (i)
253 PsVs are optically less well-resolved (which increases the distance of a PsV to CD151) and (ii) this time
254 point in particular is likely to be overcorrected for background association (see legend of
255 Supplementary Figure 3). Despite of these uncertainties, the data shows that PsVs establish contact
256 to CD151 assemblies either while still in the ECM, or in the moment of leaving the ECM.

257

258 *PsV association with HS*

259 Next, we studied the association between PsVs and HS, including a reference staining for the
260 cell body as in Figure 1. However, we cannot image TMA-DPH with our STED microscope. Instead of
261 TMA-DPH, we used Itgα6 as a reference marker for the cell body as it is not detected at cell protrusions
262 (compare TMA-DPH and Itgα6 in Figure 1A). PsVs are visualized by click-chemistry and imaged in the
263 confocal channel. HS and Itgα6 were stained by antibodies without prior permeabilization, and imaged
264 at STED microscopic resolution. The three stainings were simultaneously recorded.

265 As shown in Figure 5A (green), the Itgα6 staining results in a densely spotted pattern. The
266 Itgα6 intensity does not change over time (Supplementary Figure 4E). The pattern of the HS staining
267 is variable regarding the overlap of HS with both, PsVs and Itgα6 (Figure 5A). Moreover, CytD
268 treatment increases the HS intensity (Figure 5B, also visual when comparing the brightness of HS in
269 Figure 5A upper and lower images). This increase of intensity is particularly notable at the 0 min time
270 point, where the samples treated with CytD have a more than two-fold higher intensity and differ
271 significantly from the control. This suggests that CytD prevents loss of HS occurring during or after PsV
272 translocation.

273 In the control, the PCC between PsVs and HS is close to zero (Figure 5C, for control PCC values
274 of flipped images see Supplementary Figure 4). The largest PCC is found at 0 min/CytD, which reflects
275 the finding that at this time point both PsVs and HS preferentially locate at the cell periphery.
276 However, over time the accumulated PsVs diminish by translocating to the cell surface, which is
277 accompanied by the PCC decreasing to zero, the same value as in the control (Figure 5C). Additionally,

278 we analyze the PCC between PsVs and HS specifically in the cell body region, excluding the cell
279 periphery (Figure 5D). The PCC in the cell body region is close to zero for the control. After CytD, we
280 observe a trend towards a higher PCC between 0 min and 30 min. The fraction of PsVs tightly
281 associating with HS at 0 min is increased by more than 3-fold by the CytD treatment. Over the next
282 180 min, the fraction decreases until it reaches the control value (Figure 5E).

283 Altogether, the analysis of the PCC between HS and PsVs (Figure 5C) and the fraction of tightly
284 HS associated PsVs (Figure 5E) shows that CytD increases at 0 min the HS/PsV association, because
285 PsVs remain accumulated in the ECM. After CytD removal, this association is lost, only in the region of
286 the cell body is a trend towards a higher PCC at 30 min (Figure 5D) that could reflect HS-coated virions
287 translocating to the cell surface.

288 Next, we plot for each PsV their distance to the next nearest Itg$\alpha$6 maximum against the
289 distance to their next nearest HS maximum. In the control, the distances remain unchanged over the
290 entire observation time; 59% - 65% of the PsVs have a short distance (< 250 nm) to both Itg$\alpha$6 and HS
291 (Figure 6B, black; see also Supplementary Table 1), and another 12 - 15% a short distance (< 250 nm)
292 to HS but not to Itg$\alpha$6 (> 250 nm) (Figure 6B, green). The distance plots shown in Figure 6C are in line
293 with the observation that the distance patterns of PsVs in untreated cells do not change over the
294 180 min observation time (Figure 6C, please compare the upper distance plots from left to right). In
295 cells treated with CytD, a larger fraction of PsVs is accumulated at the periphery at the 0 min time
296 point, as marked by a larger fraction (46% as opposed to 12% in the control; Figure 6B, green) of PsVs
297 with a short distance (< 250 nm) to HS and a large distance (> 250 nm) to Itgα6. Over time, the PsVs
298 in the CytD treated cells (Figure 6C, lower row) acquire a shorter distance to Itgα6 and a larger distance
299 to HS. After 180 min, the distances are similar to the untreated control.

300 If HS would bind irreversibly to PsVs, the population with short HS-PsV distances is expected
301 to be constant. However, we observe that this population diminishes. This can only be explained by
302 HS uncoating. In fact, between 60 min/CytD and 180 min/CytD, the fraction of PsVs with a large
303 distance (> 250 nm) to HS and a short distance (< 250 nm) to Itg$\alpha$6, representing PsVs at the cell body
304 without HS, increases from 9.6% to 25.2% (Figure 6B, pink). The observation that PsVs lose their HS
305 coat after translocating to the cell surface is also supported by the lower HS intensity in the control
306 (Figure 5B) and the transient increase in the PCC between HS and PsVs in the cell body at 30 min
307 (Figure 5D).

308 The movement of HS towards the cell body is demonstrated by a shortening of the HS-Itgα6
309 distance over time (Supplementary Figure 4D). Moreover, the PCC between PsVs and HS in the cell
310 body area increases (Figure 5D). Altogether, the data suggest that HS-coated PsVs migrate towards
311 the cell body. A majority of translocating PsVs shed HS within one hour after washing off of CytD

312 (Figure 6C, lower panels, showing increasing PsV-HS distances). This is the time window where we
313 notice the occurrence of endocytic PsV/CD151 structures (see above and Supplementary Figure 1).
314
315
316 **Discussion**
317 In this study, we investigate the early stages of HPV16 infection that occur prior to virus
318 endocytosis. Our findings reveal that the dynamics of actin in filopodia, rather than the diffusion of
319 released particles, are crucial for the release of viruses from the adhesive ECM and their subsequent
320 transfer to the cell body. When actin-dependent processes are inhibited, virus particles remain
321 trapped in the ECM, allowing for a more synchronized observation of the infection process. Upon
322 removing the transfer blockade, we observe a rapid translocation of heparan sulfate (HS)-coated virus
323 capsids from the ECM to CD151 assemblies and the cell body. Subsequently, the capsid sheds its HS
324 coat and is endocytosed in association with CD151.
325
326 *A reversible block of PsV translocation from the ECM to the cell body by CytD*
327 Many viruses use cell surface HS for primary attachment, including herpes simplex virus
328 type 1, human cytomegalovirus, human immunodeficiency virus type 1, adenovirus type 2, dengue
329 virus, hepatitis B virus, and vaccinia virus (***Cagno et al., 2019***). HPVs could be different as they bind as
330 well to HS of the extracellular basement membrane, at least *in vivo* during the wounding and healing
331 processes required for infection (***Day and Schelhaas, 2014; Kines et al., 2009; Schiller et al., 2010***).
332 For studying the translocation of virions from the ECM to the cell surface, we arrest the
333 translocation with the actin-transport inhibitor CytD. After 5 h, we find a 6-fold increase of PsVs in the
334 cell periphery compared to the control (Figure 2B). After washing off of CytD, the accumulated PsVs
335 diminish with a half-time of about 15 min. This demonstrates fast translocation of PsVs to the cell
336 surface, further supported by the increase in the PCC between PsVs and CD151 from 0 min to 30 min
337 (Figure 3C).
338 Infectivity is diminished by 30% (Figure 1E) when cells are allowed to recover for 19 h after
339 washing off of CytD and PsVs. In comparison to the control, this effect appears moderate, considering
340 that the 5 h incubation time without CytD allows for continuous infection by the PsVs. In addition,
341 slightly harmful effects of the CytD treatment cannot be excluded. The rapid onset of PsV translocation
342 and the moderate effect on infection indicate that CytD only transiently prevents PsV uptake.
343 It is possible that accumulated PsVs are merely diminished by the wash off, however, the
344 effect of this could not have been very strong, considering the 6-fold accumulation of PsVs after the
345 5 h incubation with CytD. Moreover, in Figure 4C, we measure the diminishment of accumulated PsVs

346 in the cell border region, in this case as percentage of all PsVs. The diminishment in the cell border
347 does not reciprocally reflect an increase of PsVs at the cell body. However, assuming that those PsVs
348 not in the cell border region nor within the boundaries of the cell are not increasing, we conclude that
349 over time the number of PsVs at the cell body increases. Hence, the PsV diminishment at the cell
350 border region is accompanied by an increase of cell body PsVs (provided background PsVs are
351 constant), documenting that PsVs indeed translocate.

352 Compared to Figure 2B, in Figure 4C the half-time of diminishment appears longer. We
353 attribute this to an underestimation of the number of PsVs at 0 min/CytD. If the resolution of the
354 accumulated PsVs in Figure 4C had been higher, their fraction might have been larger than 36%.
355 Consequently, the half-time of PsV diminishment would be shorter yet. In contrast, the microscope
356 resolution in Figure 2 is not a limiting factor for the time course measurements, as instead of counting
357 PsVs (Figure 4C) we quantify their integrated fluorescence intensity (only possible at the periphery, as
358 autofluorescence precludes quantification of PsVs in the cell body region). Despite of these minor
359 uncertainties, we conclude that the translocation step is fast and efficient.

360 Some trends in the data suggest that the CytD treatment synchronizes HPV uptake. On the
361 one hand, we see endocytic structures after CytD treatment more frequently (for examples see
362 Supplementary Figure 1), in particular between 60 min and 180 min. On the other hand, the CD151
363 intensity diminishes over time only after the CytD treatment (Figure 3B). We speculate that the
364 processing of the PsVs in the ECM promotes desynchronization and is largely completed after the 5 h
365 pre-incubation with CytD. Hence, after CytD removal most PsVs are ready at the same time for cell
366 surface binding. Compared to the control, 6-fold more PsVs (Figure 2B) synchronously translocate to
367 the cell surface. Thus, in the following 3 h more endocytic events occur than in the control, which is
368 noticeable in a diminishment of CD151 being co-internalized with the PsVs.

369

370 *The role of actin-driven virion transport*

371 As outlined above, the electrostatic HPV-HS bond is strong, and thus requires processing of
372 the capsid surface/HS in order to proceed on the infection pathway. This hypothesis is supported by
373 several studies showing that e.g., the activity of HS cleaving enzymes facilitates the virus release from
374 the ECM and infection (***Surviladze et al., 2015***). CytD supposedly does not inhibit the activity of these
375 enzymes that may be present in the ECM (***Jamieson et al., 2021***). It is possible that not at every ECM
376 location all enzymes are available, therefore PsVs must be pulled through the ECM to the required
377 enzymes. If that is the case, CytD is indeed not likely to inhibit the processing enzymes, but rather
378 inhibits the transport of PsVs and thus prevents the contact to the necessary enzymes. Alternatively,
379 processing might be completed but virions remain associated with the ECM by electrostatic/van-der-

380 Waals forces. In this case, for ECM release actin-driven transport would be required to transport the
381 virion out of the sticky matrix to the cell surface. Here, detachment from the ECM may be facilitated
382 by new bonds established between the PsVs and cell surface receptors. Now, the PsVs and cell surface
383 receptors move towards the central cell body by intracellular dynamics and we ultimately observe
384 endocytosis (see Figure 3A).

385 In our experiments, many PsVs reach the cell body after crossing a distance of several
386 micrometers (see the analyzed cell periphery area in Figure 2A). It has been previously described that
387 HPV-PsVs are taken up from the ECM via transport along actin-rich protrusions (***Schelhaas et al., 2008;***
388 ***Smith et al., 2008***). In HeLa cells, the speed of the fastest, straight migrating PsVs is in the range of
389 several micrometer per minute (***Schelhaas et al., 2008***). Considering that only the fastest PsVs move
390 at that speed, we propose our observed time course is in accordance with the previously reported
391 migration of PsVs along actin-rich protrusions.

392 If cells require some time to recover from CytD before PsV migration restarts, the
393 translocation half-time of 15 min is likely to be overestimated. In any case, the translocation is fast
394 compared to the entire infection process and therefore cannot largely contribute to the asynchronous
395 HPV uptake.

396 Inhibition of transport diminishes infection only of subconfluent but not of confluent HaCaT
397 cells by about 50% (***Schelhaas et al., 2008***). Therefore, actin-dependent translocation along
398 protrusions may be dispensable for infection at a high cell density (***Schelhaas et al., 2008***) and simply
399 increases the exposure of cells to virions (***Smith et al., 2008***). However, this increased exposure could
400 be relevant *in vivo*, as wounding of the epidermis results in upregulation of filopodia formation
401 (***Vasioukhin et al., 2000***). Filipodia usage not only facilitates infection but also increase the likelihood
402 of virions to reach their target cells during wound healing, the filopodia-rich basal dividing cells. In
403 fact, several viruses exploit filopodia during virus entry (***Chang et al., 2016***), wherefore actin-driven
404 virion transport could have a more important role in HPV infection than currently assumed.

405

406 *Translocating PsVs are decorated with HS which they lose over time*

407 At 0 min/CytD, 15% of the PsVs are tightly associated with HS (Figure 5E), i.e. the distance
408 between PsVs and HS is ≤ 80 nm. 80 nm is above the theoretical distance between an HS fragment
409 adhering to the surface of a PsV and the PsV position. Considering the important role of HS as a primary
410 attachment site, the fraction of 15% appears unexpectedly small. One factor contributing to an
411 underestimation is that accumulated PsVs are not well-resolved (see above). Therefore, some PsV
412 maxima positions actually represent the positions of several merged PsV maxima. Instead of several
413 correct positions that may be within a distance of 80 nm to HS, we obtain a displaced position further

414 away from HS and then these PsVs would not only not contribute to the fraction of tightly associated
415 PsVs, but increase the fraction of non-tightly associated PsVs. This error decreases over time, as the
416 accumulated PsVs diminish and individual PsVs become better resolved. Another reason for
417 underestimation could be that the HS antibody does not reach all HS epitopes in the dense matrix, or
418 that PsV binding and antibody binding to HS is to some extent mutually exclusive. Finally, not all PsVs
419 bound to the ECM are expected to bind to HS but could also bind to laminin 332 (***Culp et al., 2006***).
420 The shortening of the HS-Itgα6 distance (Supplementary Figure 4D) suggests movement of HS
421 towards the cell body. Moreover, in CytD treated cells, after 30 min, the increase in the PCC between
422 PsVs and HS specifically measured in the cell body region (Figure 5D) implies co-migration of PsVs and
423 HS. PsV-HS association decreases in 180 min from 15% to 5% (Figure 5E), with 5% being equal to the
424 association in the control (Figure 5E). Hence, over time PsVs lose their HS coat. Loss of HS is also visible
425 in Figure 6C, showing that over time more PsVs have very long distances to HS. Additionally, the lower
426 HS intensity level in the control (Figure 5B) suggests that those PsVs that are actively taken up lose
427 their HS coat. These observations are in line with a previous study showing that the colocalization of
428 HS with cell surface and endocytosed virions decreases over time unless virions are directed into a
429 non-infectious entry pathway (***Selinka et al., 2007***).
430 In conclusion, as previously postulated by others (***Ozbun and Campos, 2021***), our data
431 confirms that PsVs released from the ECM are decorated with HS. However, they lose HS within a few
432 hours after translocation, perhaps due to further structural changes of the capsids or when they bind
433 to receptors for endocytosis.
434
435 *PsVs-CD151 association is an early contact to the cell surface*
436 CD151 is crucial for cell entry (***Scheffer et al., 2013; Spoden et al., 2008***). Hence, PsVs must
437 establish contact to CD151 assemblies sometime between the first cell surface contact and
438 endocytosis. As shown in Figure 3D, about 10% of the PsVs are tightly associated with CD151 over the
439 entire incubation period if cells are not treated with CytD. We find a similar effect in samples treated
440 with CytD, with the exception of the 0 min/CytD time point, where the value of associated PsVs is
441 almost halved. The reduction could be in some part due to background overcorrection (see legend of
442 Supplementary Figure 3), but also mainly because not all PsVs have translocated via actin-driven
443 transport to CD151 receptor assemblies.
444 In any case, the data suggest that PsVs establish contact to CD151 assemblies at the moment
445 of translocation to the cell surface, and from then on, the fraction of tightly associated PsVs remains
446 on a 10% level. This implies that, after the initial formation of the PsV-CD151 assemblies, they do not
447 change in nature. Yet, we observe agglomerated CD151 maxima with PsVs at later time points that

448 likely are endocytic structures (see arrow in Figure 3A, Supplementary Figure 1). Therefore, some
449 further CD151 reorganization into larger entry platforms must occur (***Florin and Lang, 2018***). This is in
450 accordance with the observation that virions enter the cell in crowds with many of them occupying
451 one endocytic organelle (***Schelhaas et al., 2012***). However, we do not resolve these events in our
452 assay, either because they are too rare or they are not associated with a change in the PsV-CD151
453 distance.

454 For the PsVs tightly associated with CD151, one may have expected a larger fraction than 10%.
455 Aside from the issues regarding the PsV-HS association, for the PsV-CD151 association our 80 nm
456 distance criteria may be too strict, because PsVs are not expected to bind directly to CD151 but to
457 larger plasmalemmal assemblies containing, among other proteins, the yet unknown PsV cell surface
458 receptor.

459 Altogether, we propose that the initial contact between PsVs and the cell surface involves an
460 assembly defined by CD151 (Figure 7). Moreover, our data show that after cell surface contact the
461 virions are decorated with HS fragments.

462

463 *Integration of our data into the cascade of steps underlying HPV infection*

464 HPV infection is the result of several steps, starting with the initial binding of virions via
465 electrostatic and polar interactions (***Dasgupta et al., 2011***) to the primary attachment site HS, which
466 induces capsid modification (***Feng et al., 2024***) and HS cleavage (***Surviladze et al., 2015***), enabling the
467 virion to be released from the ECM or the glycocalyx. Next, virions bind to the cell surface (to a
468 secondary receptor or an early version of it), and become internalized via endocytosis, before they are
469 trafficked to the nucleus (***Ozbun and Campos, 2021***).

470 We propose that after 5 h of CytD treatment, glycan-induced structural activation of the
471 capsid and HS cleavage essentially are completed ((i) in Figure 7). Subsequently, (ii) the HS-decorated
472 virion is transported from the ECM to the cell body on filopodia, which takes about 15 min. During this
473 process, PsV-CD151 association occurs early. (iii) In the samples recorded 30 – 180 min after CytD
474 wash off, we observe that PsVs lose their HS coat, and individual PsV-CD151 assemblies seem to merge
475 into larger structures that are subsequently endocytosed.

476

477

478 **Materials and Methods**

479 *Antibodies and PsVs*

480 We used the following primary antibodies in immunostainings. For the capsid protein L1, a
481 rabbit polyclonal antibody (pAb) K75 (1:1000) as described previously (***Rommel et al., 2005***), for

482 CD151 a mouse monoclonal antibody (mAb) (1:200) (Biorad, cat# MCA1856GA), for Heparan sulfate
483 (HS) a mouse IgM monoclonal antibody (1:200) (amsbio, cat# 370255-S) and for Itgα6 a rabbit
484 polyclonal antibody (1:200) (Invitrogen™, cat# PA5-12334). As secondary antibodies we used a STAR
485 GREEN-coupled goat-anti-rabbit (1:200) (Abberior, cat# STGREEN-1002-500UG), an AlexaFluor™ 594-
486 coupled donkey-anti-rabbit (1:200) (Invitrogen™, cat# A21207), an AlexaFluor™ 594-coupled donkey-
487 anti-mouse (1:200) (Invitrogen™, cat# A21203), an AlexaFluor™ 594-coupled donkey-anti-mouse IgM
488 (1:200) (Invitrogen™, cat# A21044), a STAR RED-coupled goat-anti-mouse (1:200) (Abberior, cat#
489 STRED-1001-500UG) and a STAR RED-coupled goat-anti-rabbit (1:200) (Abberior, cat# STRED-1002-
490 500UG). Additionally, phalloidin iFluor488 (1:1000 of ready to use solution) (abcam, cat# ab176753)
491 or phalloidin iFluor647 (1:1000) (abcam, cat# ab176759) was used to stain F-actin. Staining of the PsV
492 plasmid DNA was performed by click-labeling according to the manufacturer's instructions with the
493 dye 6-FAM Azide (Baseclick EdU 488 kit, Carl Roth, cat# 1Y67.1).
494 HPV16 PsVs were produced following established procedures (***Buck et al., 2004; Spoden et***
495 ***al., 2012***). HEK293TT cells were cultured in 175 cm² flasks and transfected with polyethylenimine (PEI),
496 using equimolar amounts of codon-optimized HPV16 L1/L2 (pShell 16L1/L2wt) and a reporter plasmid
497 (pGL4.20-puro-HPV16 LCR). For the production of 5-ethynyl-2'-deoxyuridine (EdU)-labeled PsVs, the
498 culture medium was replaced 5 hours post-transfection with fresh medium containing 30 µM EdU.
499 After 48 hours, cells were harvested, centrifuged, and washed twice with phosphate-buffered saline
500 (PBS) supplemented with 9.5 mM $MgCl_2$ (1x PBS/ $MgCl_2$). Following a final centrifugation step, the
501 pellet was resuspended in 1x PBS/ $MgCl_2$ containing 0.5% Brij58 (Sigma-Aldrich), and 0.2% Benzonase
502 (Merck Millipore), and incubated for 24 hours at 37°C on a rotating platform. Subsequently, lysates
503 were chilled on ice and the NaCl concentration was adjusted to 0.85 M. After clarification by
504 centrifugation, the supernatant was loaded onto an iodixanol (Optiprep) gradient consisting of 39%,
505 33%, and 27% layers (bottom to top). Gradients were equilibrated for 90 minutes at room temperature
506 before ultracentrifugation at 55,000 rpm for 3.5 hours at 16°C. Fifteen fractions of 300 µl each were
507 collected from the top and analyzed via luciferase reporter assay to identify peak fractions. PsV titers
508 were determined based on packaged genomes (viral genome equivalents, vge) as previously described
509 (***Spoden et al., 2012***). The concentrations of stock solutions are 7,7 x $10^6$ vge/µl (for microscopy
510 experiments) and 14,1 x $10^6$ vge/µl (for the luciferase assay).
511
512 *Cell culture*
513 For microscopy, human immortalized keratinocytes (HaCaTs) (Cell Lines Services, Eppelheim,
514 Germany) are cultured in high glucose DMEM (Gibco®, cat# 61965-026) medium supplemented with
515 10% FBS (PAN Biotech, cat# P30-3031) and 1% Penicillin/Streptomycin (10,000 U/ml Penicillin,

516 10 mg/ml Streptomycin; PAN Biotech, cat# P06-07100) at 37 °C with 5 % $CO_2$. For the luciferase
517 infection assay, cells were grown at 37°C in Dulbecco's modified Eagle's medium (DMEM + GlutaMAX
518 (Thermo Fisher Scientific), supplemented with 10% FBS (Sigma-Aldrich), 1% minimum essential
519 medium non-essential amino acids (MEM non-essential amino acids (Thermo Fisher Scientific)), and
520 5 µg/ml ciprofloxacin (Fresenius Kabi). For experiments, the antibiotics in the medium are omitted.
521
522 *Sample preparation and immunostaining*
523 About 150,000 HaCaT cells were plated onto 25 mm diameter poly-L-lysine (PLL) coated glass
524 coverslips in 6-well plates and incubated for 24 h at 37°C and 5% $CO_2$. The next day, cells were
525 incubated at 37°C and 5% $CO_2$ for 5 h with PsVs (50 vge/plated cell) and 10 µg/ml cytochalasin D (CytD;
526 stock solution 10 mg/ml in dimethyl sulfoxide (DMSO)) (Life Technologies, cat# PHZ1063) in DMEM
527 supplemented with 10% FBS. For controls, we added the same amount of DMSO without CytD. Cells
528 were washed with PBS (137 mM NaCl, 2.7 mM KCl, 1.76 mM $KH_2PO_4$, 10 mM $Na_2HPO_4$, pH7.4) and
529 fresh DMEM supplemented with 10% FBS was added. Cells were incubated further at 37°C and 5% $CO_2$
530 for 0 min (here the medium was added followed by immediate removal), 15 min, 30 min, 60 min and
531 180 min. Cells were washed twice with PBS and fixed at room temperature (RT) with 4% PFA in PBS
532 for 30 min, unless membrane sheets are generated. In this case, the coverslips were placed in ice cold
533 sonication buffer (120 mM KGlu, 20 mM KAc, 10 mM EGTA, 20 mM HEPES, pH 7.2) and a 100 ms
534 ultrasound pulse at 100% power was applied. This was repeated until in total about 10 pulses are
535 applied at different locations of the coverslip. Then, membrane sheets were fixed like cells at RT with
536 4% PFA in PBS for 30 min. PFA is removed, and residual PFA is quenched by 50 mM $NH_4Cl$ in PBS for
537 30 min. Afterwards, samples are blocked with 3% BSA in PBS for 30 min. Staining of PsVs was
538 performed by click-labeling with the dye 6-FAM for 30 min at RT according to the manufacturer's
539 instructions. Then, samples were washed three times with PBS. In case of no PsV labeling by click-
540 chemistry, directly after blocking, the respective primary antibodies are added: mouse IgM mAb
541 against HS (1:200), rabbit pAb against Itgα6 (1:200), mouse mAb against CD151 (1:200) and rabbit pAb
542 K75 against L1 (1:1000) in 3% BSA in PBS for 2 h. Samples were washed three times with PBS before
543 adding the respective secondary antibodies and fluorescent labelled phalloidins in 3% BSA in PBS for
544 1 h: for HS we add AlexaFluor™ 594 coupled to donkey-anti-mouse IgM (1:200), for Itgα6 STAR RED
545 coupled to goat-anti-rabbit (1:200), for CD151 AlexaFluor™ 594 coupled to donkey-anti-mouse (1:200)
546 or STAR RED coupled to goat-anti-mouse (1:200), for L1 AlexaFluor™ 594 coupled to donkey-anti-
547 rabbit (1:200) or STAR GREEN coupled to goat-anti-rabbit (1:200) and for F-actin phalloidin iFluor488
548 (1:1000) or phalloidin iFluor647 (1:1000). Afterwards, samples are washed three times with PBS,

549 followed by mounting of the coverslips onto microscopy slides using ProLong® Gold antifade mounting
550 medium (Invitrogen, cat# P36930).
551
552 *Confocal and STED microscopy*
553 For confocal and STED microscopy, samples were imaged employing a 4-channel STED
554 microscope from Abberior Instruments (available at the LIMES institute imaging facility, Bonn,
555 Germany). The microscope is based on an Olympus IX83 confocal microscope equipped with an
556 UPlanSApo 100x (1.4 NA) objective (Olympus, Tokyo, Japan). Confocal and STED micrographs are
557 recorded simultaneously. For confocal imaging, a 485 nm laser is used for the excitation of 6-FAM,
558 STAR GREEN and phalloidin iFluor488, and emission is detected at 500–550 nm. For STED imaging, a
559 561 nm laser (at 45%) is used for the excitation of AlexaFluor™ 594 (detection at 580–630 nm) and a
560 640 nm laser (at 45%) for the excitation of STAR RED and phalloidin iFluor647 (detection at 650-
561 720 nm), in combination with a 775 nm laser for depletion (at 45%). The pixel size is set to 25 nm.
562
563 *Analysis of confocal and STED micrographs*
564 Images are analyzed using Fiji ImageJ in combination with a custom written macro, essentially
565 as described previously (***Schmidt et al., 2024***). When analyzing double stainings of Alexa594 (red
566 channel) and STAR RED (long red channel), we corrected for crosstalk from the red into the long red
567 channel by subtracting 40% of the intensity of the red channel image from the long-red channel image.
568 First, images are smoothed with a Gaussian blur to improve maxima detection. For confocal
569 PsV-DNA micrographs, we employed a Gaussian blur of $\sigma = 1$, and for confocal PsV-L1 and STED
570 micrographs a Gaussian blur of $\sigma = 0.5$. Local maxima were detected using the 'Find Maxima' function
571 (noise tolerance 60 for L1 if stained together with phalloidin iFluor488, and 80 if stained together with
572 CD151, 3 for click-labeled PsVs, 8 for CD151, 6 for HS and 15 for Itgα6), yielding maxima positions in
573 pixel positions. For analysis, rectangular regions of interest (ROIs) are defined. To measure the L1
574 maxima intensity (Figure 1C and D) the ROIs covered the whole image. For CytD wash off experiments
575 the rectangular ROIs covered mainly the cell body (75%) but included the cell periphery as well (25%).
576 In order to define the cell border region (Figure 4B), the ImageJ 'Make Binary' function is used
577 on CD151 STED micrographs for generating a binary mask. When possible, the 'Wand' tool is used to
578 further outline the area covered by the cell, otherwise the same was done manually using the original
579 micrograph as a reference. From the outline in the binary mask, a ROI is created, that is then filled in
580 white with the 'Flood Fill' Tool. The ROI is shrunk by 20 pixels, and cleared inside, what leaves a
581 20 pixels broad, closed ribbon marking (i) the intracellular side of the cell and (ii) arbitrary edges
582 produced in the process above. These edges are removed by manual adjustments with the 'Pencil'

583 tool and the clear function. Afterwards, the remaining border region defines the intracellular side of
584 the cell border. From this border region a ROI is created by applying the 'Wand' tool, that is
585 symmetrically broadened to 40 pixels. From the 40 pixels, 30 pixels cover the intracellular and 10 pixels
586 the extracellular side. Using the ImageJ 'Find Maxima' function, PsV-L1 maxima are detected (at a
587 noise tolerance of 80) both in the cell border region ROI and in a ROI covering the entire micrograph.
588 From these values, the percentage of PsVs within the cell border region is calculated.

589 For measuring e.g. the CD151 intensity over time, we used ROIs as illustrated in
590 Supplementary Figure 2A, and measured in the ROI the mean gray value. For background correction,
591 we subtracted the mean gray value measured in a ROI next to the cell.

592 For measuring maxima intensity, a ROI with a diameter of 125 nm (5 pixels) was placed onto
593 the determined maxima positions (see above). Using these ROIs, the average mean gray value of each
594 maximum is measured. The average background mean gray value is measured in a ROI placed next to
595 the cell and subtracted from the average mean gray value of the maxima.

596 To measure the shortest distance, e.g. between PsV and CD151 maxima, as a quality control
597 for the PsV maxima (CD151 maxima do not undergo the quality control step) we placed onto each
598 maximum position a horizontal and a vertical linescan (31 pixels long × 3 pixels width). Afterwards, we
599 fitted a Gaussian distribution to the intensity distribution of each maximum. Only if at least one of the
600 fits exhibits a fit quality of $R^2 > 0.8$ and if the Gaussian maximum locates central to the intensity
601 distribution the maximum is included in the further analysis. Moreover, using a 125 nm ROI at the PsV
602 and CD151 maxima positions, the center of mass of fluorescence is determined, yielding the maxima
603 positions in sub-pixels. Based on these positions we further calculated the shortest distance of a PsV
604 maximum to the nearest CD151 maximum.

605 Using the shortest distances, we either calculated the fraction of tightly associated PsVs over
606 time (the fraction of PsVs with a distance ≤ 80 nm to e.g. CD151), or the average shortest distance
607 over time. The fraction of tightly associated PsVs is further corrected for random background
608 association. Random background association increases with the maxima density. The relationship
609 between background association and maxima density is expressed in a linear calibration line. For the
610 calibration line, we use the same images and determine the fraction of PsVs with a distance to e.g.
611 CD151 measured on horizontally and vertically flipped (randomized) ROI-defined images (see also
612 Supplementary Figure 2A). The fraction is plotted against the maxima density. Fitting of a linear
613 regression line yields the mathematical relationship between the fraction of tightly associated PsVs
614 and maxima density, from which we obtain the value to be subtracted for background correction.

615 The Pearson correlation coefficient (PCC) was calculated with a custom written ImageJ macro
616 in ROIs as illustrated in e.g. Supplementary Figure 2A. As a control we performed the analysis on

617 horizontally and vertically flipped ROI-defined images as well (see e.g. Supplementary Figure 2A). The
618 cell body PCC between PsVs and HS is measured in smaller ROIs covering exclusively the cell body
619 region (this is confirmed with the Itgα6 image as reference).
620 Per condition and biological replicate, 14 - 15 images are analyzed. For images from one set
621 of experiments, in the figure the same channels are shown at the same scaling and same lookup-
622 tables.
623
624 *Epi-fluorescence microscopy and image analysis*
625 For epifluorescence microscopy, we used microscopic equipment and settings as previously
626 described (***Homsi et al., 2014***) except of the illumination system, which is replaced by a Lumencor
627 Light engine® Spectra 90-10034 (Lumencor, USA). In brief, PFA-fixed cells are imaged in PBS containing
628 TMA-DPH [1-(4-tri-methyl-ammonium-phenyl)- 6-phenyl-1,3,5-hexatriene-p-toluenesulfonate (T204;
629 Thermofisher)] for visualizing the membranes in the blue channel. PsVs, HS and Itgα6 were imaged in
630 the green, red and far-red channels, respectively.
631 For analysis, rectangular ROIs of ≈ 45 x $10^3$ pixel are placed onto the cell body such that one
632 half of the ROI covers roughly the ECM area and the other one the cell body. The cell periphery is
633 defined using the TMA-DPH image from which a binary mask is created. With reference to the binary
634 mask, a band of 30 pixels width is created beginning at the cell body and reaching out towards the cell
635 periphery. Using this ROI, in the PsV-DNA image the size of the ROI and the mean grey values are
636 measured from which the integrated intensities are calculated after background correction.
637
638 *Luciferase infection assay*
639 HaCaT cells are grown in 24-well plates and allowed to adhere overnight. The following day,
640 cells are treated with HPV16 PsVs at a concentration of 100 vge per cell, in the presence or absence
641 of 10 µg/ml cytochalasin D (CytD) in DMSO or an equivalent amount of DMSO (control). In one
642 condition, PsVs/CytD are applied for 5 hours, after which the medium is replaced with fresh medium
643 lacking the compounds, and incubation is continued for additional 19 hours (in total 24 h). In another
644 condition, cells are exposed to PsVs/CytD continuously for the full 24 h period. Then, cells are washed
645 with PBS and lysed using 1 x Cell Culture Lysis Reagent (Promega, cat# E153A). Following high-speed
646 centrifugation, luciferase activity in the cleared lysates is quantified using an LB 942 Tristar 3
647 luminometer (Berthold Technologies). Cytotoxic effects, accompanied by a loss of membrane integrity
648 (indicated by released lactate dehydrogenase (LDH)), are determined by measuring the LDH levels in
649 the cell lysates. LDH activity is assessed using the CytoTox-ONE™ Homogeneous Membrane Integrity

650 Assay (Promega, cat# G7891). LDH fluorescence is quantified according to the manufacturer's
651 instructions using the LB 942 Tristar 3 luminometer.
652
653 *Statistics*
654 Data sets were based on three biological replicates, including 14 - 15 images per replicate. For
655 infection assay, data sets were based on three biological replicates, with three technical replicates
656 from each biological replicate. Data was tested for significance with a two-tailed, unpaired
657 student's *t* test with significance * = $p < 0.05$, ** = $p < 0.01$ and *** = $p < 0.001$.
658
659
660 **Acknowledgement**
661 LF and TL were funded by the Deutsche Forschungsgemeinschaft (DFG, German Research Foundation),
662 Projektnummer 322863883, FL696/3-2 (LF); LA 1272/8-2 (TL).
663
664
665 **References**
666
667 **Baker TS**, Newcomb WW, Olson NH, Cowsert LM, Olson C, Brown JC. 1991. Structures of bovine and
668 human papillomaviruses. Analysis by cryoelectron microscopy and three-dimensional image
669 reconstruction. *Biophysical journal* **60**:1445–1456. doi: 10.1016/S0006-3495(91)82181-6.
670 **Becker M**, Greune L, Schmidt MA, Schelhaas M. 2018. Extracellular Conformational Changes in the
671 Capsid of Human Papillomaviruses Contribute to Asynchronous Uptake into Host Cells. *Journal of*
672 *virology* **92**. doi: 10.1128/jvi.02106-17.
673 **Bruening J**, Lasswitz L, Banse P, Kahl S, Marinach C, Vondran FW, Kaderali L, Silvie O, Pietschmann T,
674 Meissner F, Gerold G. 2018. Hepatitis C virus enters liver cells using the CD81 receptor complex
675 proteins calpain-5 and CBLB. *PLoS Pathogens* **14**:e1007111. doi: 10.1371/journal.ppat.1007111.
676 **Buck CB**, Pastrana DV, Lowy DR, Schiller JT. 2004. Efficient intracellular assembly of papillomaviral
677 vectors. *Journal of virology* **78**:751–757. doi: 10.1128/jvi.78.2.751-757.2004.
678 **Cagno V**, Tseligka ED, Jones ST, Tapparel C. 2019. Heparan Sulfate Proteoglycans and Viral
679 Attachment: True Receptors or Adaptation Bias? *Viruses* **11**. doi: 10.3390/v11070596.
680 **Chang K**, Baginski J, Hassan SF, Volin M, Shukla D, Tiwari V. 2016. Filopodia and Viruses: An Analysis
681 of Membrane Processes in Entry Mechanisms. *Frontiers in microbiology* **7**:300.
682 doi: 10.3389/fmicb.2016.00300.
683 **Christiansen IK**, Sandve GK, Schmitz M, Dürst M, Hovig E. 2015. Transcriptionally active regions are
684 the preferred targets for chromosomal HPV integration in cervical carcinogenesis. *PloS one*
685 **10**:e0119566. doi: 10.1371/journal.pone.0119566.
686 **Culp TD**, Budgeon LR, Marinkovich MP, Meneguzzi G, Christensen ND. 2006. Keratinocyte-secreted
687 laminin 5 can function as a transient receptor for human papillomaviruses by binding virions and
688 transferring them to adjacent cells. *Journal of virology* **80**:8940–8950. doi: 10.1128/JVI.00724-06.

689 **Dasgupta J**, Bienkowska-Haba M, Ortega ME, Patel HD, Bodevin S, Spillmann D, Bishop B, Sapp M,
690 Chen XS. 2011. Structural basis of oligosaccharide receptor recognition by human papillomavirus.
691 *The Journal of biological chemistry* **286**:2617–2624. doi: 10.1074/jbc.m110.160184.
692 **Day PM**, Schelhaas M. 2014. Concepts of papillomavirus entry into host cells. *Current opinion in*
693 *virology* **4**:24–31. doi: 10.1016/j.coviro.2013.11.002.
694 **Doorbar J**, Quint W, Banks L, Bravo IG, Stoler M, Broker TR, Stanley MA. 2012. The biology and life-
695 cycle of human papillomaviruses. *Vaccine* **30 Suppl 5**:F55-70. doi: 10.1016/j.vaccine.2012.06.083.
696 **Dziduszko A**, Ozbun MA. 2013. Annexin A2 and S100A10 regulate human papillomavirus type 16
697 entry and intracellular trafficking in human keratinocytes. *Journal of virology* **87**:7502–7515.
698 doi: 10.1128/JVI.00519-13.
699 **Earnest JT**, Hantak MP, Park J-E, Gallagher T. 2015. Coronavirus and influenza virus proteolytic
700 priming takes place in tetraspanin-enriched membrane microdomains. *Journal of virology*
701 **89**:6093–6104. doi: 10.1128/JVI.00543-15.
702 **Evander M**, Frazer IH, Payne E, Qi YM, Hengst K, McMillan NA. 1997. Identification of the alpha6
703 integrin as a candidate receptor for papillomaviruses. *Journal of virology* **71**:2449–2456.
704 doi: 10.1128/JVI.71.3.2449-2456.1997.
705 **Feng Y**, van Bodegraven D, Kádek A, L B Munguira I, Soria-Martinez L, Nentwich S, Saha S, Chardon F,
706 Kavan D, Uetrecht C, Schelhaas M, Roos WH. 2024. Glycan-induced structural activation softens
707 the human papillomavirus capsid for entry through reduction of intercapsomere flexibility. *Nature*
708 *communications* **15**:10076. doi: 10.1038/s41467-024-54373-0.
709 **Finke J**, Mikuličić S, Loster A-L, Gawlitza A, Florin L, Lang T. 2020. Anatomy of a viral entry platform
710 differentially functionalized by integrins α3 and α6. *Scientific reports* **10**:5356.
711 doi: 10.1038/s41598-020-62202-9.
712 **Florin L**, Lang T. 2018. Tetraspanin Assemblies in Virus Infection. *Frontiers in immunology* **9**:1140.
713 doi: 10.3389/fimmu.2018.01140.
714 **Galati L**, Chiantore MV, Marinaro M, Di Bonito P. 2024a. Human Oncogenic Viruses: Characteristics
715 and Prevention Strategies-Lessons Learned from Human Papillomaviruses. *Viruses* **16**.
716 doi: 10.3390/v16030416.
717 **Galati L**, Di Bonito P, Marinaro M, Chiantore MV, Gheit T. 2024b. HPV16 Phylogenetic Variants in
718 Anogenital and Head and Neck Cancers: State of the Art and Perspectives. *Viruses* **16**.
719 doi: 10.3390/v16060904.
720 **Giroglou T**, Florin L, Schäfer F, Streeck RE, Sapp M. 2001. Human papillomavirus infection requires
721 cell surface heparan sulfate. *Journal of virology* **75**:1565–1570. doi: 10.1128/JVI.75.3.1565-
722 1570.2001.
723 **Hantak MP**, Qing E, Earnest JT, Gallagher T. 2019. Tetraspanins: Architects of Viral Entry and Exit
724 Platforms. *Journal of virology* **93**. doi: 10.1128/JVI.01429-17.
725 **Heuser J**. 2000. The production of 'cell cortices' for light and electron microscopy. *Traffic*
726 *(Copenhagen, Denmark)* **1**:545–552. doi: 10.1034/j.1600-0854.2000.010704.x.
727 **Hochdorfer D**, Florin L, Sinzger C, Lieber D. 2016. Tetraspanin CD151 Promotes Initial Events in
728 Human Cytomegalovirus Infection. *Journal of virology* **90**:6430–6442. doi: 10.1128/jvi.00145-16.
729 **Homsi Y**, Schloetel J-G, Scheffer KD, Schmidt TH, Destainville N, Florin L, Lang T. 2014. The
730 extracellular δ-domain is essential for the formation of CD81 tetraspanin webs. *Biophysical journal*
731 **107**:100–113. doi: 10.1016/j.bpj.2014.05.028.
732 **Jamieson RR**, Stasiak SE, Polio SR, Augspurg RD, McCormick CA, Ruberti JW, Parameswaran H. 2021.
733 Stiffening of the extracellular matrix is a sufficient condition for airway hyperreactivity. *Journal of*
734 *applied physiology (Bethesda, Md. : 1985)* **130**:1635–1645. doi: 10.1152/japplphysiol.00554.2020.
735 **Joyce JG**, Tung JS, Przysiecki CT, Cook JC, Lehman ED, Sands JA, Jansen KU, Keller PM. 1999. The L1
736 major capsid protein of human papillomavirus type 11 recombinant virus-like particles interacts

with heparin and cell-surface glycosaminoglycans on human keratinocytes. *The Journal of biological chemistry* **274**:5810–5822. doi: 10.1074/jbc.274.9.5810.

**Kines RC**, Thompson CD, Lowy DR, Schiller JT, Day PM. 2009. The initial steps leading to papillomavirus infection occur on the basement membrane prior to cell surface binding. *Proceedings of the National Academy of Sciences of the United States of America* **106**:20458–20463. doi: 10.1073/pnas.0908502106.

**Knappe M**, Bodevin S, Selinka H-C, Spillmann D, Streeck RE, Chen XS, Lindahl U, Sapp M. 2007. Surface-exposed amino acid residues of HPV16 L1 protein mediating interaction with cell surface heparan sulfate. *The Journal of biological chemistry* **282**:27913–27922. doi: 10.1074/jbc.m705127200.

**Martel C** de, Plummer M, Vignat J, Franceschi S. 2017. Worldwide burden of cancer attributable to HPV by site, country and HPV type. *International journal of cancer* **141**:664–670. doi: 10.1002/ijc.30716.

**Mikuličić S**, Finke J, Boukhallouk F, Wüstenhagen E, Sons D, Homsi Y, Reiss K, Lang T, Florin L. 2019. ADAM17-dependent signaling is required for oncogenic human papillomavirus entry platform assembly. *eLife* **8**. doi: 10.7554/eLife.44345.

**Ozbun MA**, Campos SK. 2021. The long and winding road: human papillomavirus entry and subcellular trafficking. *Current opinion in virology* **50**:76–86. doi: 10.1016/j.coviro.2021.07.010.

**Peng GE**, Wilson SR, Weiner OD. 2011. A pharmacological cocktail for arresting actin dynamics in living cells. *Molecular biology of the cell* **22**:3986–3994. doi: 10.1091/mbc.E11-04-0379.

**Rommel O**, Dillner J, Fligge C, Bergsdorf C, Wang X, Selinka H-C, Sapp M. 2005. Heparan sulfate proteoglycans interact exclusively with conformationally intact HPV L1 assemblies: basis for a virus-like particle ELISA. *Journal of medical virology* **75**:114–121. doi: 10.1002/jmv.20245.

**Scheffer KD**, Gawlitza A, Spoden GA, Zhang XA, Lambert C, Berditchevski F, Florin L. 2013. Tetraspanin CD151 mediates papillomavirus type 16 endocytosis. *Journal of virology* **87**:3435–3446. doi: 10.1128/JVI.02906-12.

**Schelhaas M**, Ewers H, Rajamäki M-L, Day PM, Schiller JT, Helenius A. 2008. Human papillomavirus type 16 entry: retrograde cell surface transport along actin-rich protrusions. *PLoS Pathogens* **4**:e1000148. doi: 10.1371/journal.ppat.1000148.

**Schelhaas M**, Shah B, Holzer M, Blattmann P, Kühling L, Day PM, Schiller JT, Helenius A. 2012. Entry of human papillomavirus type 16 by actin-dependent, clathrin- and lipid raft-independent endocytosis. *PLoS Pathogens* **8**:e1002657. doi: 10.1371/journal.ppat.1002657.

**Schiller JT**, Day PM, Kines RC. 2010. Current understanding of the mechanism of HPV infection. *Gynecologic oncology* **118**:S12-7. doi: 10.1016/j.ygyno.2010.04.004.

**Schmidt SC**, Massenberg A, Homsi Y, Sons D, Lang T. 2024. Microscopic clusters feature the composition of biochemical tetraspanin-assemblies and constitute building-blocks of tetraspanin enriched domains. *Scientific reports* **14**:2093. doi: 10.1038/s41598-024-52615-1.

**Selinka H-C**, Florin L, Patel HD, Freitag K, Schmidtke M, Makarov VA, Sapp M. 2007. Inhibition of transfer to secondary receptors by heparan sulfate-binding drug or antibody induces noninfectious uptake of human papillomavirus. *Journal of virology* **81**:10970–10980. doi: 10.1128/jvi.00998-07.

**Selinka H-C**, Giroglou T, Sapp M. 2002. Analysis of the infectious entry pathway of human papillomavirus type 33 pseudovirions. *Virology* **299**:279–287. doi: 10.1006/viro.2001.1493.

**Smith JL**, Lidke DS, Ozbun MA. 2008. Virus activated filopodia promote human papillomavirus type 31 uptake from the extracellular matrix. *Virology* **381**:16–21. doi: 10.1016/j.virol.2008.08.040.

**Spoden G**, Freitag K, Husmann M, Boller K, Sapp M, Lambert C, Florin L. 2008. Clathrin- and caveolin-independent entry of human papillomavirus type 16--involvement of tetraspanin-enriched microdomains (TEMs). *PloS one* **3**:e3313. doi: 10.1371/journal.pone.0003313.

785 **Spoden G**, Kühling L, Cordes N, Frenzel B, Sapp M, Boller K, Florin L, Schelhaas M. 2013. Human
786 papillomavirus types 16, 18, and 31 share similar endocytic requirements for entry. *Journal of*
787 *virology* **87**:7765–7773. doi: 10.1128/jvi.00370-13.
788 **Spoden GA**, Besold K, Krauter S, Plachter B, Hanik N, Kilbinger AFM, Lambert C, Florin L. 2012.
789 Polyethylenimine is a strong inhibitor of human papillomavirus and cytomegalovirus infection.
790 *Antimicrobial agents and chemotherapy* **56**:75–82. doi: 10.1128/aac.05147-11.
791 **Surviladze Z**, Dziduszko A, Ozbun MA. 2012. Essential Roles for Soluble Virion-Associated Heparan
792 Sulfonated Proteoglycans and Growth Factors in Human Papillomavirus Infections. *PLoS*
793 *Pathogens* **8**:e1002519. doi: 10.1371/journal.ppat.1002519.
794 **Surviladze Z**, Sterkand RT, Ozbun MA. 2015. Interaction of human papillomavirus type 16 particles
795 with heparan sulfate and syndecan-1 molecules in the keratinocyte extracellular matrix plays an
796 active role in infection. *The Journal of general virology* **96**:2232–2241. doi: 10.1099/vir.0.000147.
797 **Vasioukhin V**, Bauer C, Yin M, Fuchs E. 2000. Directed actin polymerization is the driving force for
798 epithelial cell-cell adhesion. *Cell* **100**:209–219. doi: 10.1016/s0092-8674(00)81559-7.
799 **Woodham AW**, Da Silva DM, Skeate JG, Raff AB, Ambroso MR, Brand HE, Isas JM, Langen R, Kast
800 WM. 2012. The S100A10 subunit of the annexin A2 heterotetramer facilitates L2-mediated human
801 papillomavirus infection. *PloS one* **7**:e43519. doi: 10.1371/journal.pone.0043519.
802 **Yoon CS**, Kim KD, Park SN, Cheong SW. 2001. alpha(6) Integrin is the main receptor of human
803 papillomavirus type 16 VLP. *Biochemical and biophysical research communications* **283**:668–673.
804 doi: 10.1006/bbrc.2001.4838.
805 **Zona L**, Lupberger J, Sidahmed-Adrar N, Thumann C, Harris HJ, Barnes A, Florentin J, Tawar RG, Xiao
806 F, Turek M, Durand SC, Duong FHT, Heim MH, Cosset F-L, Hirsch I, Samuel D, Brino L, Zeisel MB, Le
807 Naour F, McKeating JA, Baumert TF. 2013. HRas signal transduction promotes hepatitis C virus cell
808 entry by triggering assembly of the host tetraspanin receptor complex. *Cell host & microbe*
809 **13**:302–313. doi: 10.1016/j.chom.2013.02.006.
810 **zur Hausen H**. 2009. The search for infectious causes of human cancers: where and why (Nobel
811 lecture). *Angewandte Chemie (International ed. in English)* **48**:5798–5808.
812 doi: 10.1002/anie.200901917.

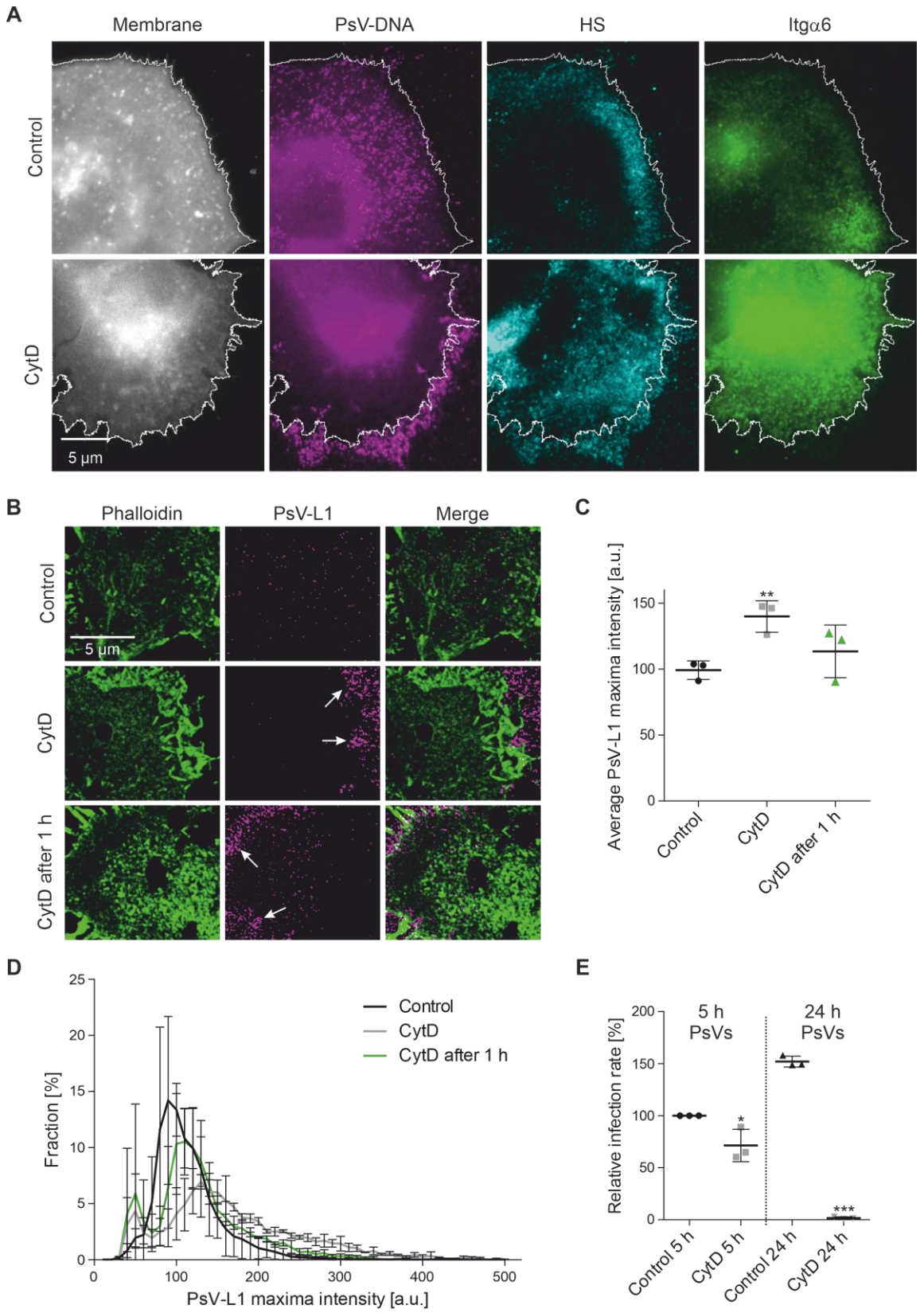


**Figure 1.** *CytD arrests PsV translocation from the ECM to the cell body.*
(A) In the absence (control) or presence of 10 µg/ml CytD, HaCaT cells are incubated with PsVs at 37 °C for 5 h. Then, cells are fixed and stained with the cell membrane dye TMA-DPH (grey). PsVs (magenta) are visualized through coupling a dye (6-FAM Azide) to the encapsidated plasmid by click-chemistry,

819 and indirect immunolabeling is used for staining of HS (AlexaFluor™ 594; cyan) and Itgα6 (STARRED;
820 green). Imaging was realized with epi-fluorescence microscopy. White lines mark the main cell body;
821 they are generated with reference to the membrane staining. (B) Same pre-treatment of cells as in (A)
822 with an additional condition where CytD is added 1 h after the PsVs (CytD after 1 h). Prior to fixation,
823 membrane sheets are generated and F-actin is stained with phalloidin iFluor488 (green) and PsVs are
824 stained by immunofluorescence using an antibody against L1 in combination with an AlexaFluor™ 594-
825 labelled secondary antibody (magenta; not shown in this figure for clarity reasons is an additional
826 staining of CD151 with STAR RED). Images of phalloidin and L1 are acquired in the confocal and STED
827 mode of a STED microscope, respectively. Arrows in the magenta panels point towards accumulated
828 PsVs. (C) Images as shown in (B) are analyzed. PsV maxima are detected and their intensities are
829 quantified in a circular 125 nm diameter region of interest (ROI), followed by background correction.
830 Values are given as means ± SD (n = 3 biological replicates; one biological replicate includes per
831 condition 14 - 15 analyzed membranes with altogether at least 1000 maxima). (D) PsV maxima
832 intensity distribution of the data in (C). The fraction of PsVs, expressed in percent, is plotted against
833 the maxima intensity. Values are given as means ± SD (n = 3). (E) HaCaT cells are treated either for 5 h
834 or 24 h with PsVs, with or without 10 µg/ml CytD. In case of the 5 h incubation, cells are washed and
835 incubated for another 19 h in medium (in total 24 h). After a total of 24 h incubation, the luciferase
836 activity of lysed cells is measured, yielding the infection rate that is normalized to LDH, resulting in the
837 normalized infection rate. The normalized infection rate is further related to the mean normalized
838 infection rate of the 5 h control, set to 100 %, yielding the relative infection rate. Values are given as
839 means ± SD (n = 3). (D) and (E). Statistical differences between control and CytD is analyzed by using
840 the two-tailed, unpaired student's *t* test (n = 3). a.u., arbitrary units.

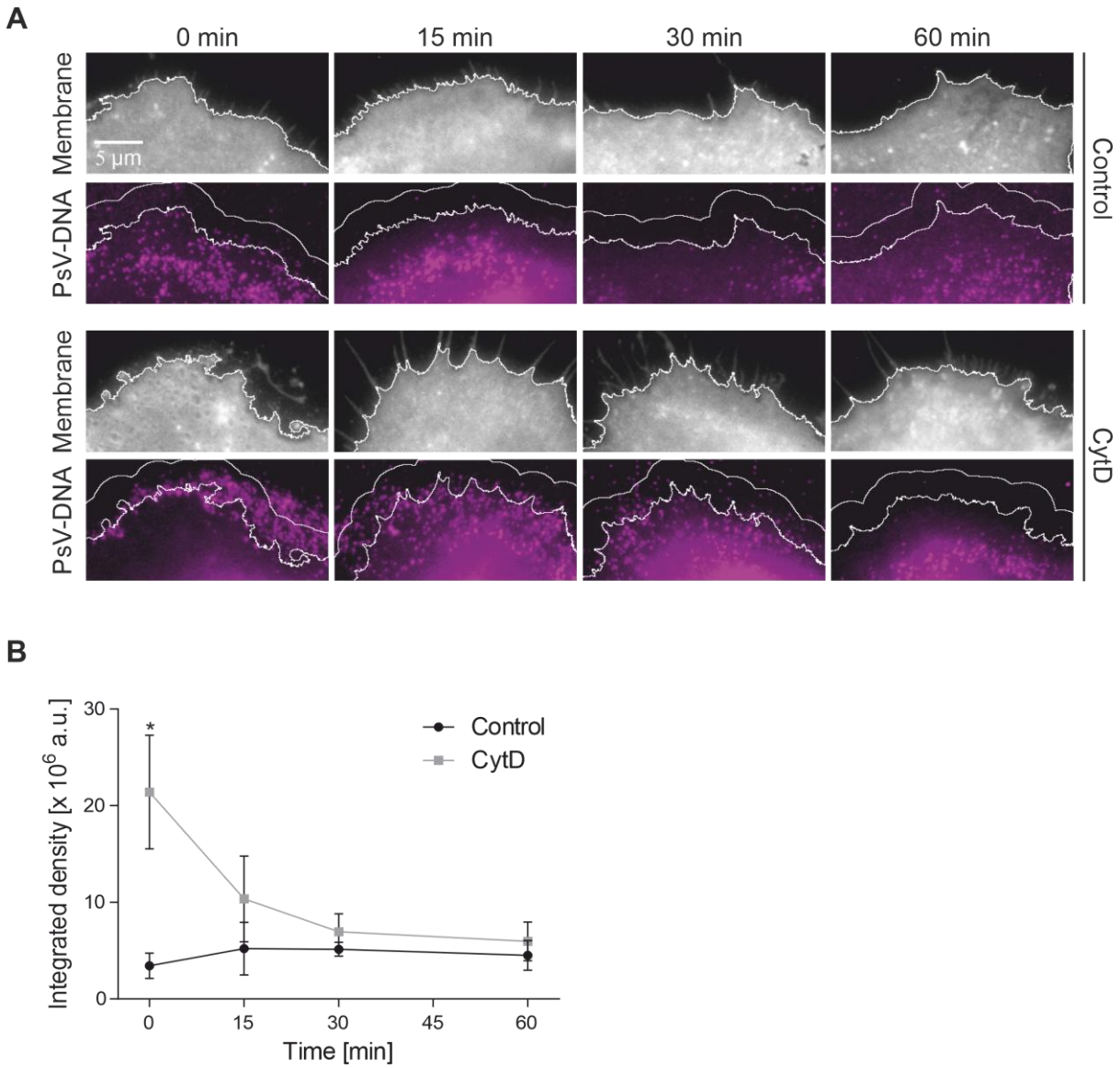


**Figure 2.** *Fast diminishment of the accumulated PsV signal from the cell periphery after washing off of CytD.*
(A) HaCaT cells are incubated with PsVs at 37 °C for 5 h, in the absence (control) or presence of CytD (10 µg/ml). Then, cells are washed and incubated for the indicated time periods without PsVs/CytD, before they are fixed and stained as in Figure 1 (t = 0 min is identical to Figure 1A; for clarity we show only the membrane (grey) and the PsV staining (magenta)). White lines in the membrane images are generated with reference to the membrane staining. One line marks the cell body. The cell body line was broadened by 30 pixels (see additional smoother white lines in the PsV channel, magenta). (B) Magenta images, the area enclosed by the two white lines mark the cell periphery. The PsV signal of the periphery is quantified as integrated density, background corrected, and plotted over time. Values are given as means ± SD. The statistical difference between the same time points of control and CytD is analyzed by using the two-tailed, unpaired student's *t* test (n = 3 biological replicates).

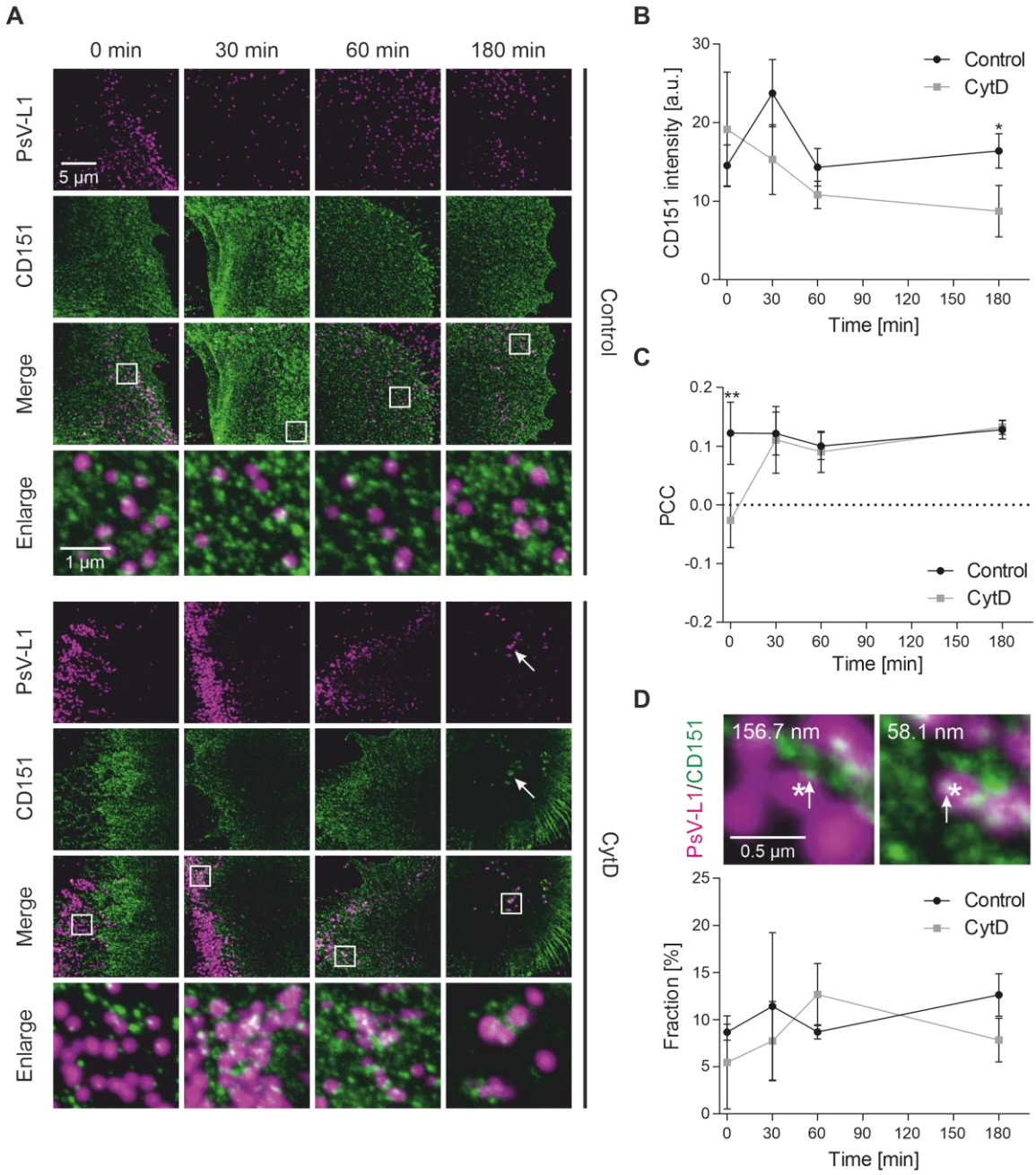


854
855 **Figure 3.** *Association between PsVs and CD151.*
856 (A) HaCaT cells are incubated with PsVs at 37 °C for 5 h, in the absence (control, upper panels) or
857 presence of 10 µg/ml CytD (CytD, lower panels). Afterwards, cells are washed and incubated without
858 PsVs/CytD further for 0 min, 30 min, 60 min or 180 min, before they are fixed and stained by indirect
859 immunofluorescence for L1 (magenta; STAR GREEN) and for CD151 (green; AlexaFluor™ 594), and for
860 F-actin by fluorescent labelled phalloidin (iFluor647; here not shown for clarity, please see Figure 4 for
861 the F-actin staining). The bottom rows show enlarged views of the merged images, from the regions
862 marked by the white boxes. PsVs (L1 staining) and F-actin are imaged in the confocal and CD151 in the
863 STED mode of a STED microscope, respectively (see enlarged views). 180 min/CytD, arrows mark
864 presumably endocytic structures in the central cell body region (for more examples see also
865 Supplementary Figure 1). For analysis, we place rectangular ROIs onto the images that cover mainly
866 the cell body but include parts of the cell periphery as well (see example in Supplementary Figure 2A).
867 (B) Within these ROIs, the average CD151 intensity is measured and plotted over time. In the same
868 ROIs, (C) the Pearson correlation coefficient (PCC) between PsV-L1 (magenta) and CD151 (green) is

869 calculated and plotted over time. (D) the fraction of PsVs (in percent) that have a distance to the next
870 neighbored CD151 maximum ≤ 80 nm, which we define as tightly associated, is plotted over time. The
871 fraction of PsVs tightly associating with CD151 is corrected for random background association (for
872 details see Supplementary Figure 3). (D) Two examples of PsVs (each marked by an asterisk) taken
873 from the 30 min/CytD (left) and 60 min/CytD (right) conditions. Number in the upper left, the shortest
874 distance between the PsV-L1 maximum and the next nearest CD151 maximum (marked by an arrow)
875 is given in nm. Values are given as means ± SD (n = 3 biological replicates). Statistical difference
876 between the same time points of control and CytD is analyzed by using the two-tailed, unpaired
877 student's *t* test (n = 3).
878

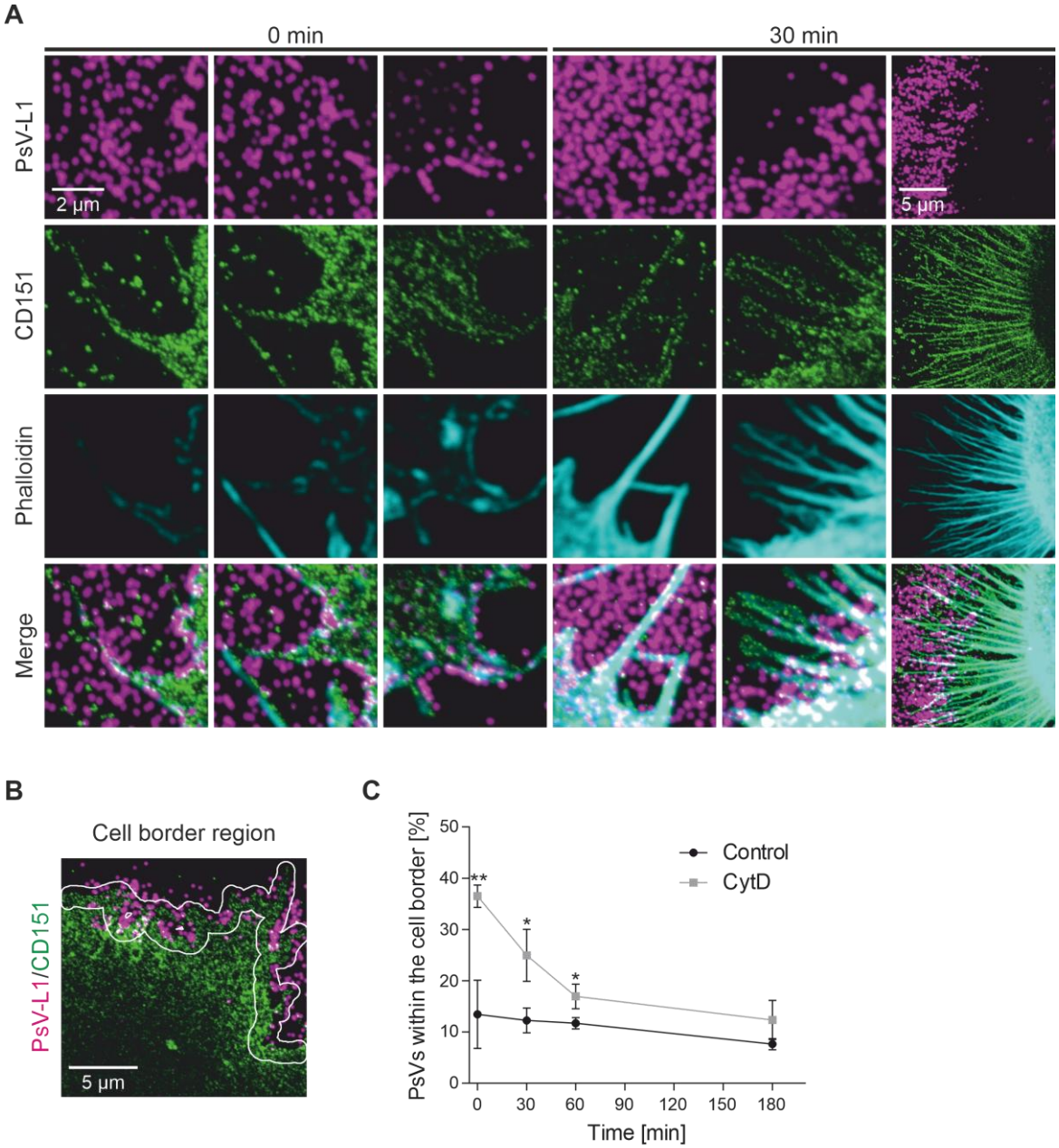


**Figure 4.** *Gallery of images illustrating the variability of filopodia/the diminishment of the number of PsVs at the cell border region after CytD removal.*
(A) Images are taken from the same experiment described in Figure 3. Many cells have filopodia. However, due to the large variability in number and shape it is impossible to show representative images. Therefore, the shown examples taken from the CytD condition are anecdotal images of cells with CD151 positive filopodia. (B) Based on the CD151 image, a cell border region is broadened to 40 pixels. Please note that this cell border region is different from the cell periphery described in Figure 2. In this analysis, the analyzed region covers both sides of the cell border (approximately 75% inside and 25% outside of the cell; for details see methods), and therefore is referred to as the cell border region. (C) Diminishment of PsV maxima from the cell border region over time, expressed as percentage of all PsVs present in the image. Values are given as means ± SD (n = 3). Statistical difference between the same time points of control and CytD is analyzed by using the two-tailed, unpaired student's *t* test (n = 3).

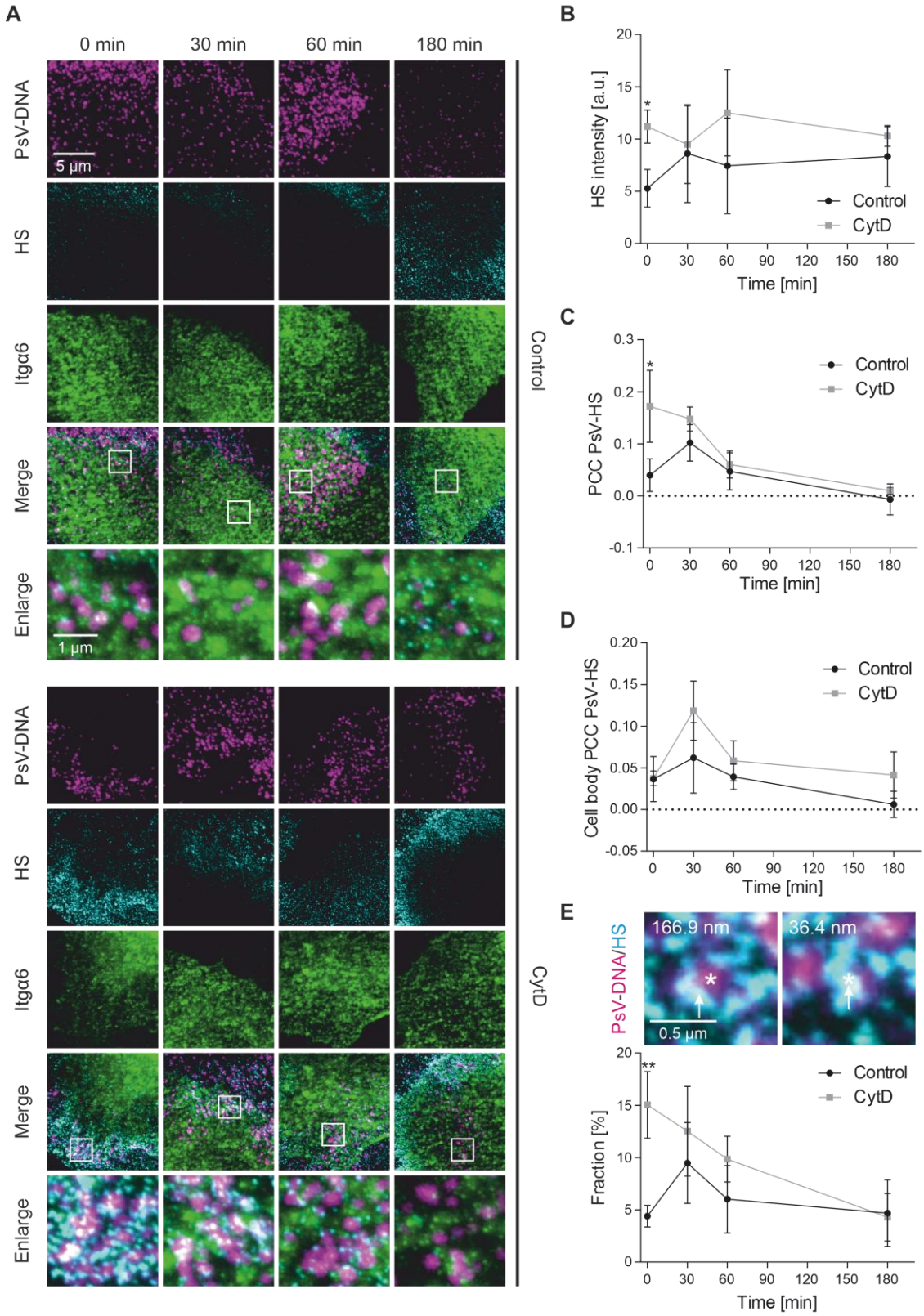


**Figure 5.** *Association between PsVs and HS.*
(A) HaCaT cells are incubated with PsVs at 37 °C for 5 h, in the absence (control, upper panels) or presence of 10 µg/ml CytD (CytD, lower panels). Afterwards, cells are washed and incubated without PsVs/CytD further for up to 180 min, before they are fixed and stained. PsVs (magenta) are visualized by click-chemistry (6-FAM Azide, see also above) and indirect immunolabeling is used for HS (cyan;

901 AlexaFluor™ 594) and for Itgα6 (green; STAR RED). Shown in the bottom rows are enlarged views of
902 the white boxes in the merged images. PsVs (DNA staining) are imaged in the confocal and HS and
903 Itgα6 in the STED mode of a STED microscope, respectively (see enlarged views). For analysis, we place
904 rectangular ROIs onto the images that cover mainly the cell body but include parts of the cell periphery
905 as well (see example in Supplementary Figure 4A) (B) Average HS intensity over time. (C) PCC between
906 PsV-DNA (magenta) and HS (cyan) over time. (D) PCC between PsV-DNA (magenta) and HS (cyan) in
907 the region of the cell body over time. (E) The fraction of PsVs (in percent) tightly associating with HS
908 (distance ≤ 80 nm) plotted over time (for background correction see Supplementary Figure 5). Two
909 examples of PsVs (each marked by an asterisk) taken from the 0 min/CytD condition. Number in the
910 upper left is the shortest distance in nm between the PsV-DNA maximum and the next nearest HS
911 maximum (marked by an arrow). Values are given as means ± SD (n = 3 biological replicates). Statistical
912 difference between the same time points of control and CytD is analyzed by using the two-tailed,
913 unpaired student's *t* test (n = 3).
914

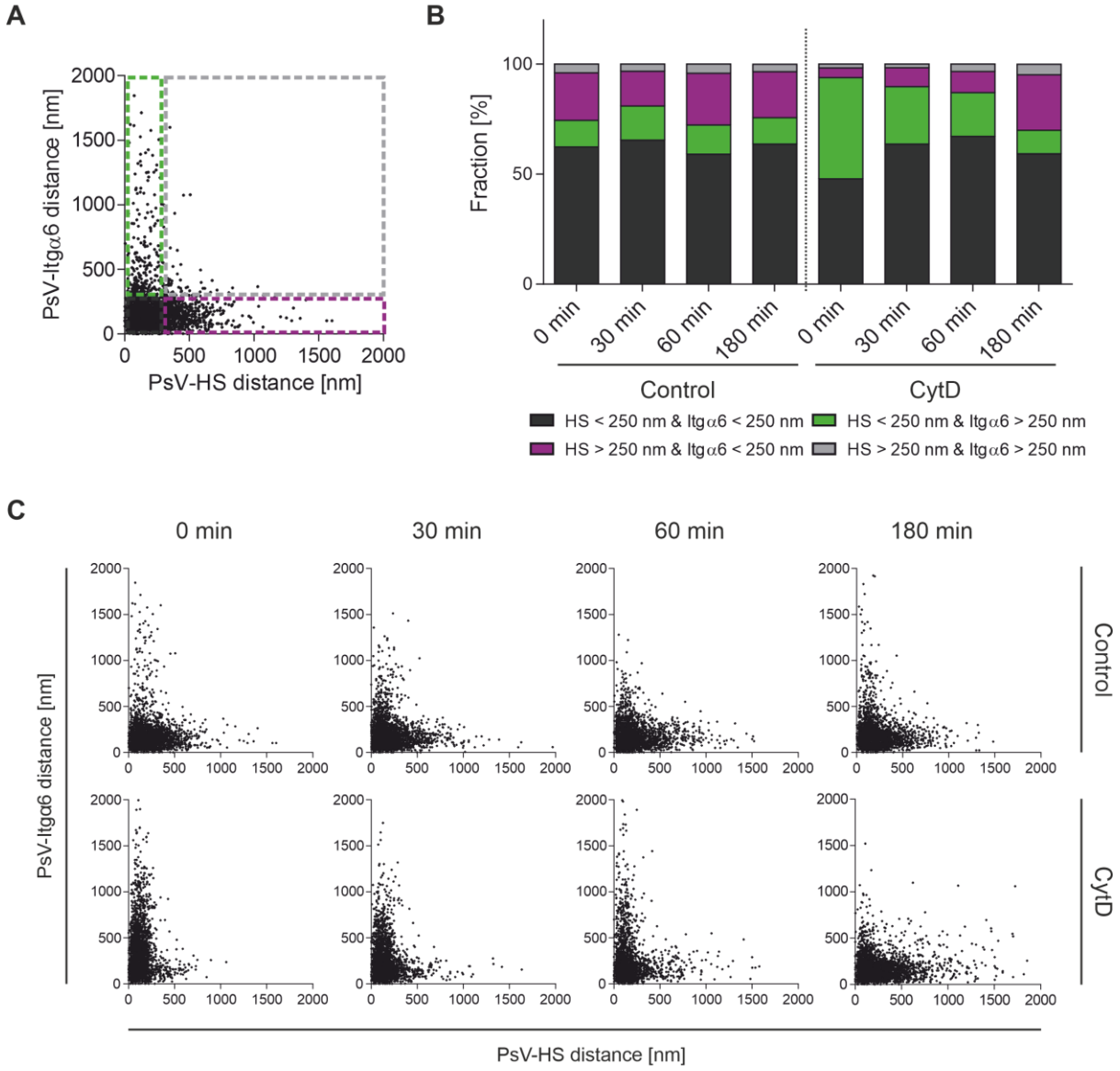


**Figure 6.** *Pattern of PsV-Itgα6 distances and PsV-HS distances over time.*
(A) Definition of four PsV populations. Dashed green rectangle; PsVs with a distance to HS < 250 nm and to Itgα6 > 250 nm. Dashed magenta rectangle; PsVs with a distance to HS > 250 nm and to Itgα6 < 250 nm. Dashed gray square; PsVs with a distance to HS > 250 nm and to Itgα6 > 250 nm. PsVs not included in the previous categories have a distance to HS < 250 nm and to Itgα6 < 250 nm. (B) Based on the experiment shown in Figure 5, the PsV fraction size (in percent) of the four populations defined in (A) is illustrated using the same colors as in (A), and using black for PsVs with a distance < 250 nm each to Itgα6 and HS. Shown is the mean of the three biological replicates. For means ± SD and statistical analysis see Supplementary Table 1. (C) The same data as in (B), plotting for each PsV the shortest distance to Itgα6 against the shortest distance to HS (pooling the three biological replicates; 3,043 – 4,080 PsVs per plot).

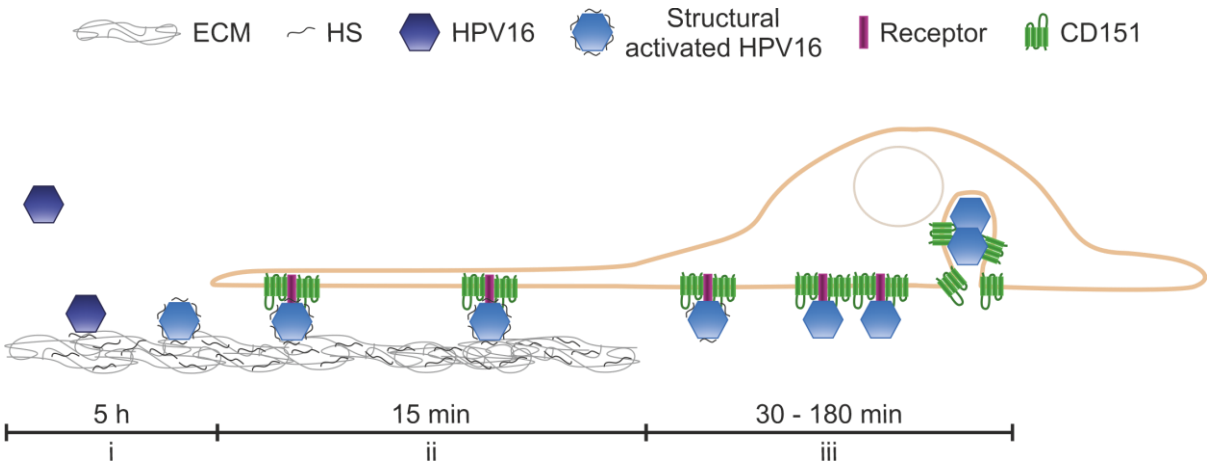


**Figure 7.** *Model figure.*
The structural activation of PsVs in the ECM is completed within 5 h (i). Within 15 min, the structurally-activated HPV16 translocate from the ECM to CD151 assemblies, likely located at the filopodia, and move toward the cell body (ii). During this process, the virions retain some heparan sulfate (HS) on their surface. (iii) Eventually, they lose their HS coat, and individual PsV-CD151 assemblies merge into larger complexes, which are subsequently endocytosed.

940 **Supplementary information**
941

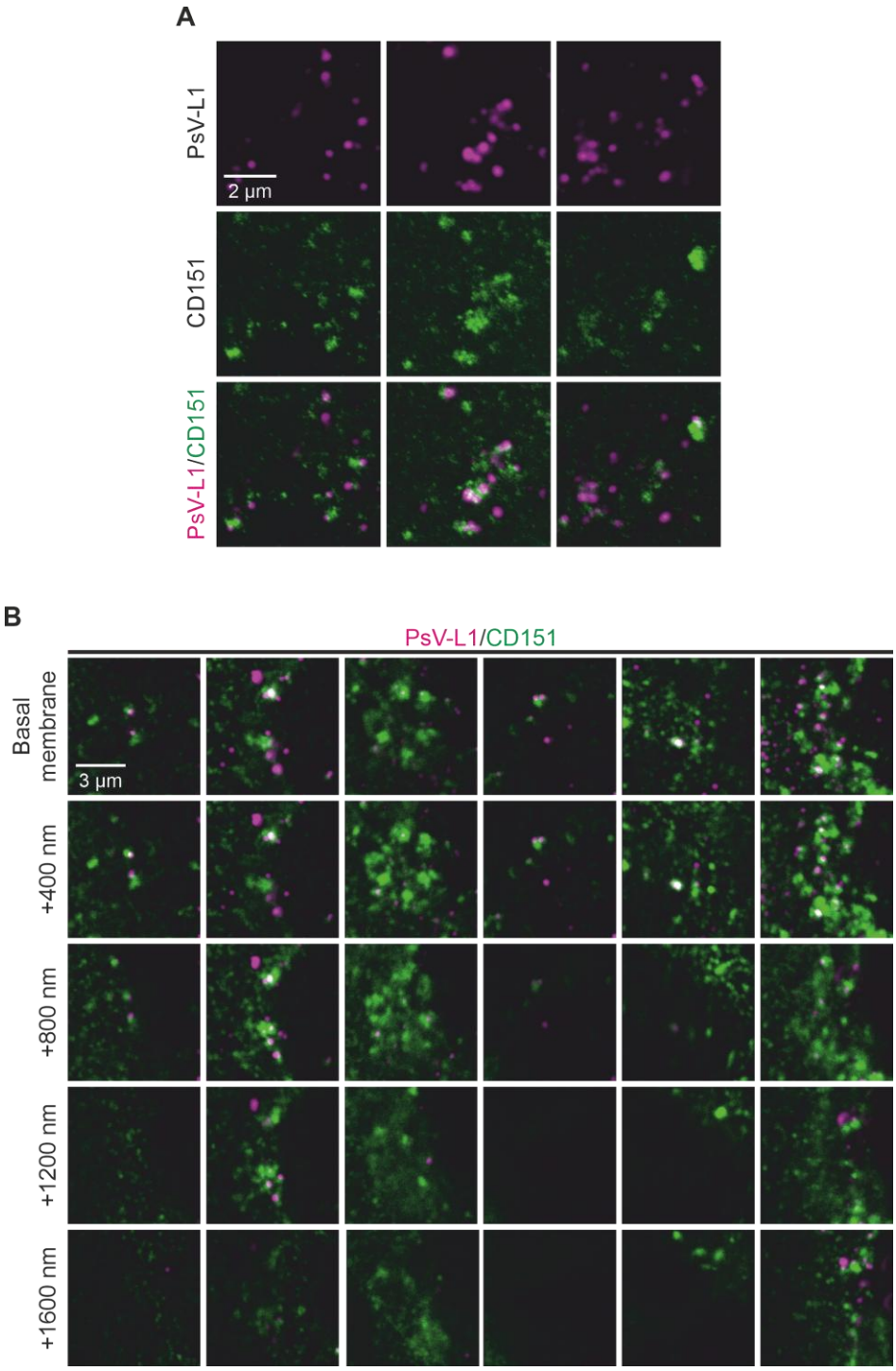


942
943
944 **Supplementary Figure 1.** *Examples of agglomerated CD151 maxima that are associated with PsVs and*
945 *presumably are endocytic structures.*
946 (A) From the data described in Figure 3 (180 min/CytD), we show more examples of agglomerated
947 CD151 maxima (see green patches) that associate with PsVs (magenta) and likely are endocytic
948 structures. (B) The same experiment as in (A), but cells are scanned with 400 nm steps in the axial
949 direction at confocal resolution, starting at the basal membrane. The structures noticed in the basal
950 membrane as agglomerated CD151 maxima continue deeper into the cell. In some cases, more than
951 a micrometer (see second example from the left).

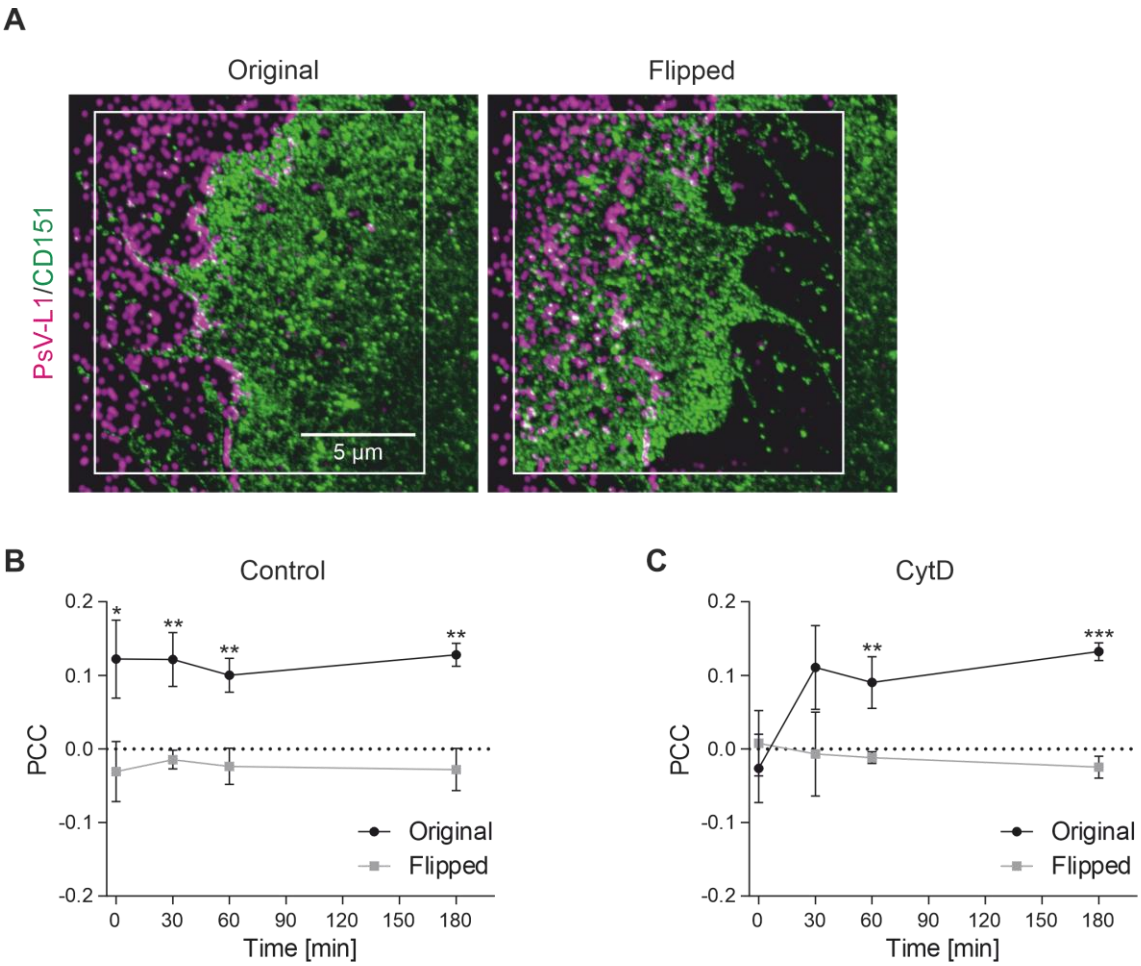


**Supplementary Figure 2.** *PCC controls.*
(A) In order to determine the background colocalization, we analyze the PCC on flipped images as well. Left, original image taken from the 0 min/CytD condition. The ROI selected for analysis is shown as white box. Right, the green image within the ROI is flipped horizontally and vertically. Now, a pair of images with the same density of objects and intensity distributions can be analyzed. (B) PCC between PsV-L1 and CD151 of the control condition (Figure 3C) is shown again, together with the respective PCCs determined on flipped images. (C) The PCC between PsV-L1 and CD151 of the CytD condition (Figure 3C) is shown again, together with the respective PCCs determined on flipped images. Statistical difference between the same time points of original and flipped images is analyzed by using the two-tailed, unpaired student's *t* test (n = 3). Values are given as mean ± SD.

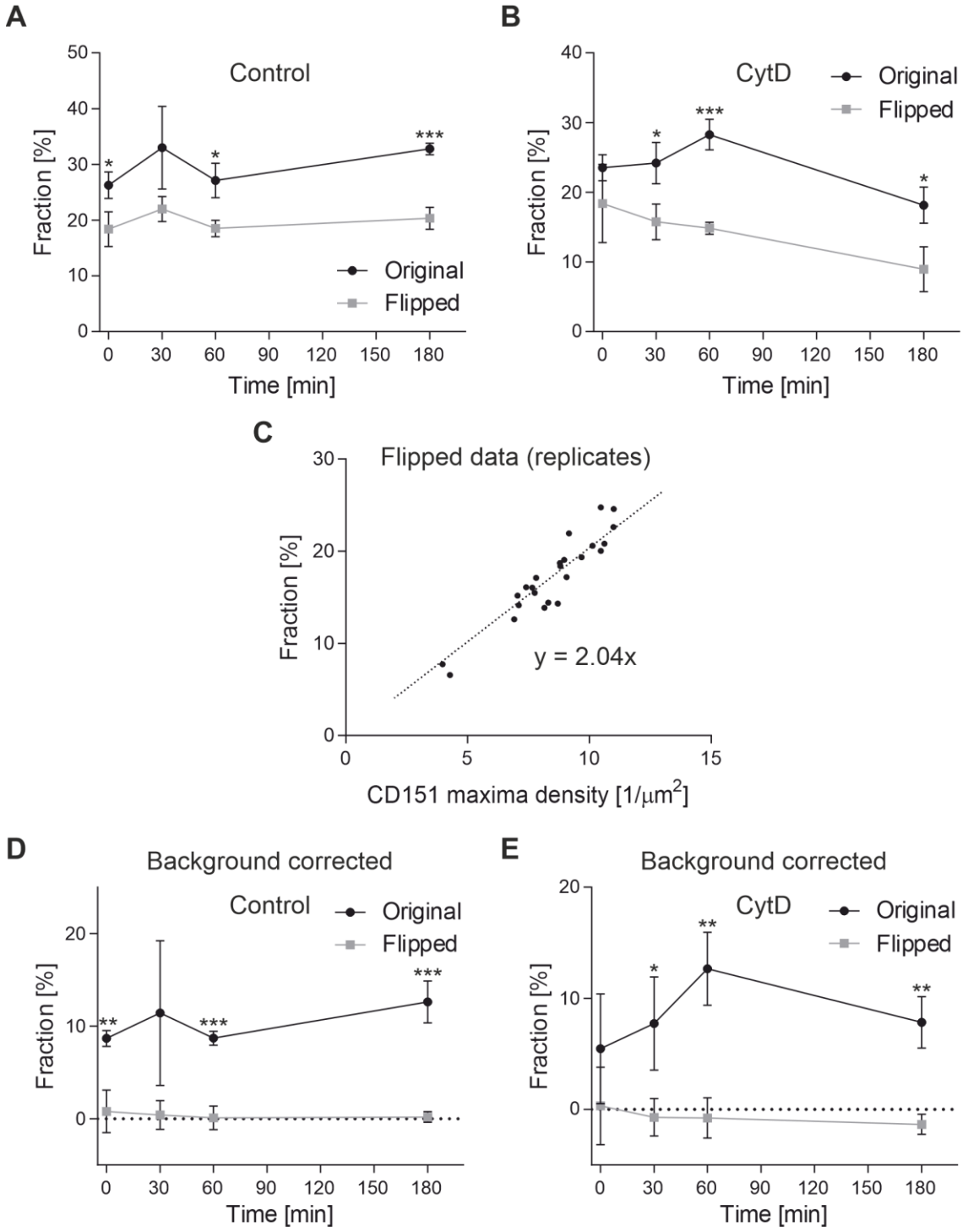


964
965 **Supplementary Figure 3.** *Background correction of the fraction of PsVs tightly associated with CD151.*
966 (A) The fraction of tightly associated PsVs (PsV-L1 maxima with a distance ≤ 80 nm to the next nearest
967 CD151 maximum) in the control of the experiment described in Figure 3, analyzed on original and
968 flipped images (for an example of a flipped image see Supplementary Figure 2A). On flipped images,
969 the fractions often are more than half of the original images. This demonstrates that many of the PsVs
970 have a distance ≤ 80 nm to CD151 merely by chance (random background association). (B) Same as
971 (A) for the CytD condition. (C) Each flipped data point in (A) and (B) is the average of three biological
972 replicates. From the altogether 24 replicates of the flipped images, we plot the fraction of tightly
973 associated PsVs against the CD151 maxima density. As expected, the fraction increases with the

974 maxima density. The fitted linear regression line describes how the background association depends
975 on the maxima density. With the equation of the regression line the random background association
976 can be calculated, for any maxima density in an original images the random background association
977 can be calculated. (D) For each replicate from the original and the flipped images in (A), the
978 background fraction is calculated using the equation of the regression line in (C) and the respective
979 CD151 maxima density, and subtracted from the fraction of tightly associated PsVs. (E) Same as (D)
980 for the CytD condition. The corrected original values in (D) and (E) are shown in Figure 3D. Please note
981 that the data point CytD/0 min likely is overcorrected because we flip a CD151 rich region onto the
982 accumulated PsVs that in the original image are in a region that is low in CD151. Statistical difference
983 between the same time points of original and flipped images is analyzed by using the two-tailed,
984 unpaired student's *t* test (n = 3). Values are given as mean ± SD.
985

986

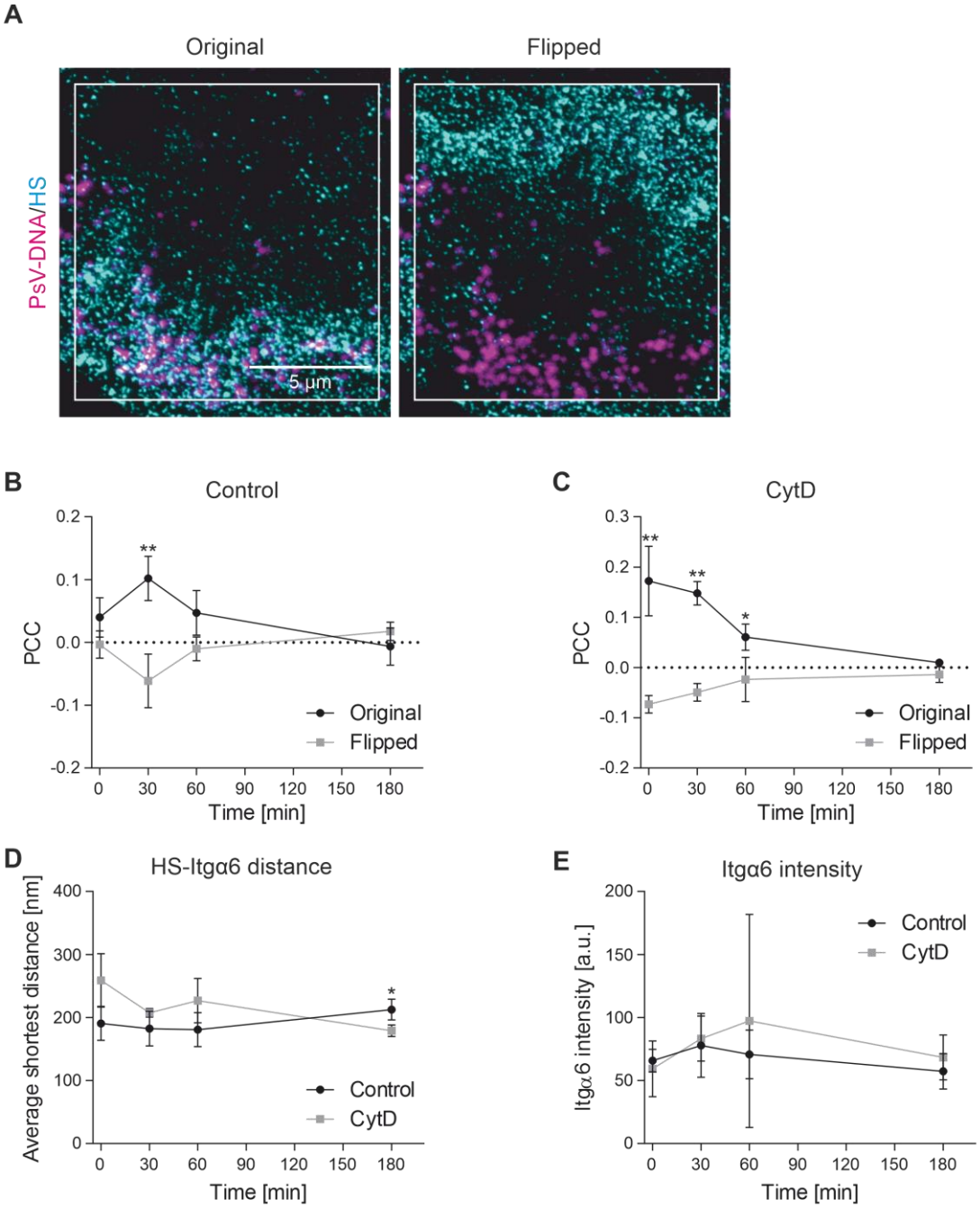


987

988 **Supplementary Figure 4.** *PCC controls, HS-Itgα6 average shortest distance and Itgα6 intensity.*
989 Additional analysis from the experiment shown in Figure 5. (A) Example of flipped HS image used as
990 control (for explanation please see legend of Supplementary Figure 2). Left, original image taken from
991 the 0 min/CytD condition. The ROI selected for analysis is shown as white box. Right, the cyan image
992 within the ROI is flipped horizontally and vertically. (B) The PCC between PsV-DNA and HS of the
993 control condition (Figure 5C) is shown again, together with the respective PCCs determined on flipped
994 images. (C) The PCC between PsV-DNA and HS of the CytD condition (Figure 5C) is shown again,
995 together with the respective PCCs determined on flipped images. (D) The average shortest distance
996 of HS maxima to the next nearest Itgα6 maximum and (F) the average Itgα6 intensity. Statistical
997 difference between the same time points of original and flipped images or control and CytD is analyzed
998 by using the two-tailed, unpaired student's *t* test (n = 3). Values are given as mean ± SD.
999

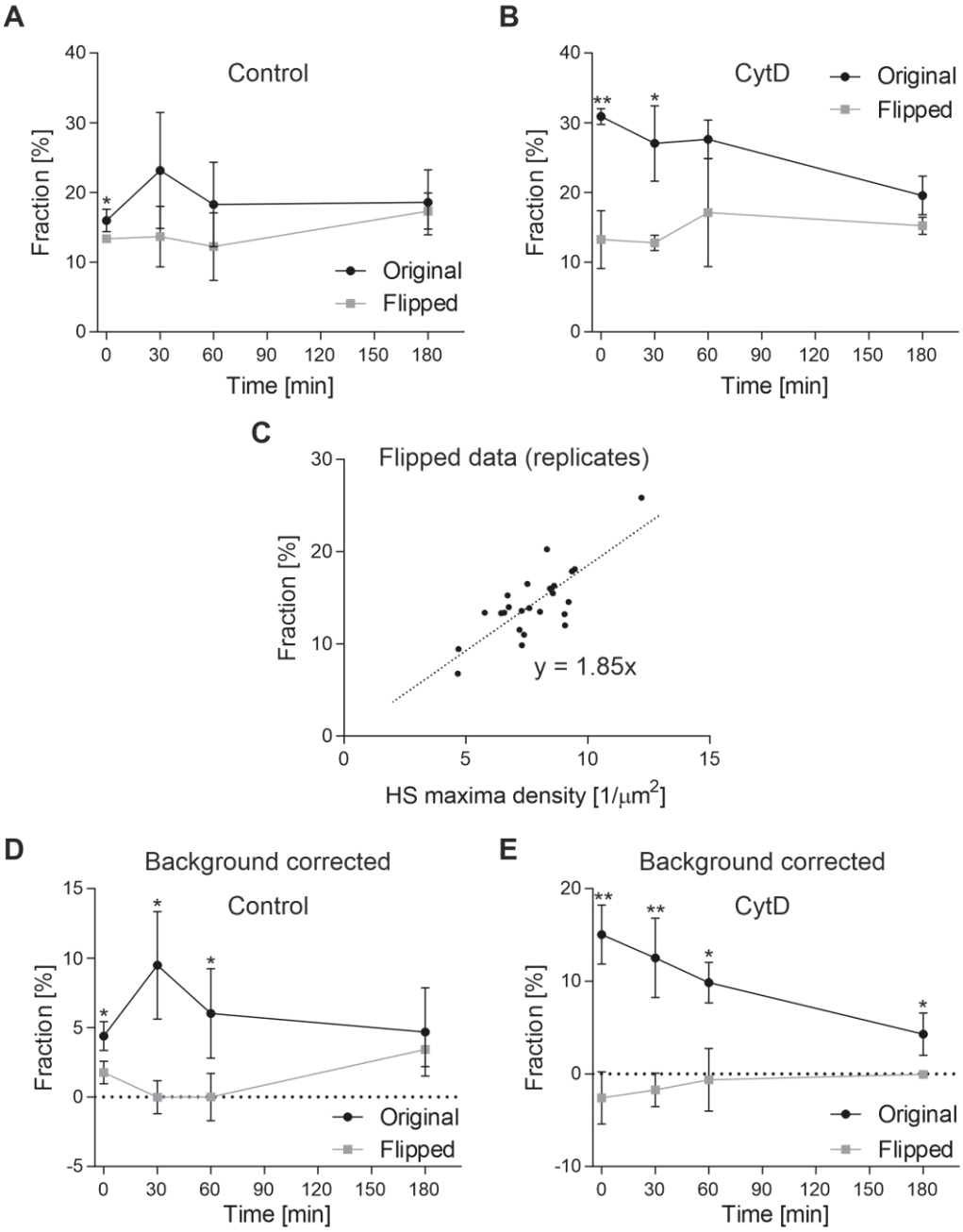


**Supplementary Figure 5.** *Background correction of the fraction of PsVs tightly associated with HS.* (A) The fraction of tightly associated PsVs (PsV-DNA maxima with a distance ≤ 80 nm to the next nearest HS maximum) in the control of the experiment described in Figure 5, analyzed on original and flipped images (for an example of a flipped image see Supplementary Figure 4A). (B) Same as (A) for the CytD condition. (C) From the altogether 24 replicates of the flipped images, the fraction of tightly associated PsVs is plotted against the HS maxima density, and a linear regression line is fitted to the data points. (D) For each replicate from the original and the flipped images in (A), the background fraction is calculated using the equation of the regression line in (C) and the respective HS maxima density, and subtracted from the fraction of tightly associated PsVs. (E) Same as (D) for the CytD condition. The background corrected original values in (D) and (E) are shown in Figure 5E. Statistical difference between the same time points of original and flipped images is analyzed using the two-tailed, unpaired student's *t* test (n = 3). Values are given as mean ± SD.

**Supplementary Table 1.** Means ± SD of the data shown in Figure 6B. P-values between control and CytD are calculated by using the two-tailed, unpaired student's *t* test (n = 3). Significant p-values are illustrated in bold.

| **Fraction of PsVs [%]** | **0 min** | | | **30 min** | | | **60 min** | | | **180 min** | | |
|---|---|---|---|---|---|---|---|---|---|---|---|---|
| | control | CytD | p-value | control | CytD | p-value | control | CytD | p-value | control | CytD | p-value |
| **HS < 250 nm & Itga6 < 250 nm** | 62.31 ± 5.05 | 47.83 ±3.26 | **0.0271** | 65.48 ± 8.35 | 63.67 ± 1.14 | 0.7764 | 59.06 ± 10.64 | 67.16 ± 9.84 | 0.4739 | 63.69 ± 4.27 | 59.28 ± 3.17 | 0.3065 |
| **HS < 250 nm & Itga6 > 250 nm** | 12.18 ± 5.51 | 46.04 ± 3.67 | **0.0019** | 15.46 ± 3.14 | 26.12 ± 2.16 | **0.0167** | 13.25 ± 1.94 | 19.87 ± 3.12 | 0.0637 | 11.97 ± 1.53 | 10.64 ± 1.15 | 0.3808 |
| **HS > 250 nm & Itga6 < 250 nm** | 21.59 ± 4.07 | 4.34 ± 0.37 | **0.0040** | 15.83 ± 5.73 | 8.58 ± 2.33 | 0.1723 | 23.49 ± 6.55 | 9.60 ± 4.81 | 0.0731 | 20.88 ± 3.31 | 25.24 ± 1.96 | 0.1842 |
| **HS > 250 nm & Itga6 > 250 nm** | 3.93 ± 0.30 | 1.79 ± 0.60 | **0.0110** | 3.23 ± 0.88 | 1.63 ± 0.21 | 0.0675 | 4.19 ± 2.43 | 3.38 ± 2.20 | 0.7425 | 3.46 ± 0.54 | 4.84 ± 2.87 | 0.5393 |